PROCESSES FOR FORMING PLASMONIC WAVEGUIDES FROM SELF-ASSEMBLED GOLD NANOPARTICLE THIN FILMS

Francis Zaato

Thesis submitted to the faculty of the
Virginia Polytechnic Institute and State University in partial fulfillment of the requirements for the degree of

Master of Science
In
Electrical Engineering

Dr. Kathleen Meehan
Dr. Ira Jacobs
Dr. Ahmad Safaai-Jazi

July 18, 2006
Blacksburg, VA

Keywords: nanoparticles, plasmonic waveguides, self-assembly.

Processes for Forming Plasmonic Waveguides from Self-assembled Gold Nanoparticle Thin Films

Francis Zaato

ABSTRACT

Miniaturization of electronic circuits and systems continue to pose great difficulties in meeting the demand and anticipated growth for information services and their associated electronics. Of the several information processing techniques under consideration for devices of the future, optical systems are considered to offer significant advantages in terms of speed and bandwidth. Unfortunately, at the dimensions of contemporary electronics, optical waveguides will fail to assist significantly due to the fact that standard optical waveguides will have dimensions below the diffraction limit and hence optical waveguiding at such scales will be impractical.

In order to circumvent this, recent work in the area of using nano-sized protrusions to guide light below the diffraction limit has been receiving a decent amount of attention. Such systems have typically involved using electron beam lithography to create these perturbations on metallic surfaces called plasmonic waveguides. While these waveguides are fairly efficient, in the amounts required to make real circuits this method would be impractically slow and prohibitively expensive.

However, such waveguides could be made much more cheaply if means could be found to arrange colloidal nanoparticles on suitable substrates. In this project, nanoscale self-assembly has been investigated with the aim of achieving such ends. Colloidal nanoparticles have been synthesized and self-assembled onto substrates such that they show near field interactions necessary for plasmonic waveguiding without any aggregation. Absorption peak shifts, which were obtained during the experimental phase of this project confirmed that such nanoparticle assemblies can be achieved and that they do demonstrate some plasmonic waveguiding action. With this first step, it is hoped that films like these may find use for quick and cheap plasmonic waveguiding sometime in the near future.

Acknowledgements

First of all I would like to thank Dr. Meehan for her invaluable guidance and support while I undertook this project. Her patience and responsiveness to my needs were instrumental in me getting this project done. I enjoyed the many discussions we had and apologize if I was too much of a bother sometimes.

I would also like to thank Dr. Jacobs who has been extremely helpful to me during my entire stay at Virginia Tech. From my first class through to serving on my committee, and various stints in between, he is without doubt one professor who has helped me get through my two seasons here in Blacksburg.

In addition, an expression of gratitude to Dr. Safaai-Jazi would be in order. I greatly appreciate his willingness to meet with me time and again and all the advice he gave me which greatly assisted with my academic journey here.

And some "thank yous" to people who helped me with the work in this thesis: to Vaibhav Jain who helped out with suggestions for ISAMs and AFM imaging, to Frank Cromer, Steve M^{c}Cartney and all others in various departments at Virginia Tech who helped in one way or another.

To my family: Thank you for your hopes, support and prayers. Thanks to my parents for their patience and support; to Diana and Eric for giving me a reason to be an example and to Natalie and Andrew for a reason to persevere. I am forever thankful.

And to a special friend who helped in no small way in making all this possible: Thank you very much!

Table of Contents

List of Figures

List of Tables

Chapter 1

Introduction

1.1 Motivation

With the advent of the information age and our digital society, there has been an increased demand on the requirements of computer systems. Thus far, this demand has been met by the frequent rate of scaling of microelectronics devices, an idea publicized by Moore [1]. In addition to smaller device sizes, increased operation speeds have conspired to make the ability to meet this scaling increasingly difficult [2]. While smaller devices enable smaller and faster integrated circuits, their smaller traces have higher resistances and often produce significant amounts of heat, which can be detrimental to operation. In addition, the higher frequencies give rise to harder-driven electrons, which produce larger fields and guiding these fields becomes increasingly difficult. All these together make the task of continuing to meet Moore's law extremely daunting with current microelectronics technologies.

A promising means of overcoming the limitations of our current microelectronic technologies is to use optical waveguides to fabricate photonic logic gates. With their higher data rates, lower loss, immunity to both electrical and optical crosstalk and wide bandwidths, they make excellent alternatives to standard semiconductor device structures. However, a fundamental issue with optical and photonic systems is one of size. The sizes of these waveguides and optical paths are constrained by the diffraction limits of the wavelengths used [3,4]. This results in devices and circuits that are much larger than their equivalents in conventional microelectronics.

On another note, recent booms in the use of optical fiber in communication systems and the attendant interest in all-optical switching for such systems creates a need for a technology that is superior to the current method of converting fiber-optic signals to electrical form and back. There are speed penalties in the conversion and this ultimately limits the level of performance at which such fiber channels can carry data. In broadband systems, the requirement that each channel must be demultiplexed before optical-to-electrical conversion causes there to be a parallelization of several devices as a result of each device's limited bandwidth in the electronic domain. This causes real estate, weight and cost penalties to the installation and maintenance of repeaters, regenerators, add/drop multiplexers and such devices on fiber-optic lines.

However, the availability of a mechanism that incorporates two vital features described above – bandwidth and size – would significantly help microelectronics continue the Moore's law trend. Fiber systems could increase efficiency and reduce cost and

nanoscale all-optical chips may become reality. Such a device, called a plasmonic waveguide, may meet this challenge. The plasmonic waveguide works on the principle that optical energy impinging upon an array of closely spaced metallic nanoparticles embedded in a dielectric matrix will travel along the array [5]. The ability to employ self-assembly of nanoparticles to create plasmonic waveguides would go a long way in making plasmonic waveguides a convenient reality.

1.2 Scope of Thesis

This work is an investigation and report on the suitability of gold nanoparticles synthesized from colloidal sources and on the applicability of two different self-assembly techniques to form plasmonic arrays and waveguides. Against that back drop, primary work shall involve fabricating such nanoparticles, aligning them into two- and three-dimensional structures and characterizing the nanoparticles and these structures with respect to the target application. Two methods that are potentially cheap and very easy to use, ionic self-assembly and diblock copolymer alignment shall be given most consideration. Finally, an analysis of the characteristics will be carried out to evaluate the suitability of the processes used over the course of this project to implement optical and logic elements. In order to facilitate understanding, explanations from the physics and chemistry involved, both qualitative and quantitative, shall be given but just enough to ensure that further results can be understood and appreciated. It shall not be the intent of this work to fully explain colloidal nanoparticles and every way they may be made; suitable chemistry texts are available for such purposes [6].

1.3 References

[1] Gordon E. Moore, “Cramming more components onto integrated circuits”, Electronics Magazine 19, April 1965

[2] Chenming Hu, “Future CMOS scaling and reliability”, Proceedings of the IEEE, Vol. 81, No. 5, May 1993

[3] Maier at al, “Observation of coupled plasmon-polariton modes of plasmon waveguides for electromagnetic energy transport below the diffraction limit”, Proceedings of SPIE, Vol. 4810

[4] J.R.Krenn, H. Ditlbacher, G. Schider, A. Hohenau, A. Leitner, F.R. Aussenegg, “Surface Plasmon micro- and nano-optics”, Journal of Microscopy, Vol. 209, Pt.3 March 2003, pg167-172

[5] S.A. Maier, P.G. Kik, H.A. Atwater, S. Meltzer, E. Harel, B. Koel, A.A.G. Requicha, “Local detection of electromagnetic energy transmitted below the diffraction limit in metallic nanoparticle plasmon waveguides”, Nature Materials, Vol. 2, April 2003

[6] M.A. Hayat, “Colloidal Gold: Principles, Methods and Applications”, Academic Press, Inc, Vol. 1-3, 1989, 1991

Chapter 2

Surface Plasmons

2.1. Introduction

The fundamental phenomenon upon which plasmonic waveguides depend is the interaction between localized surface plasmons. Localized surface plasmons arise from similar means as surface plasmon polaritons, also known in some literature as surface plasmons. A fine difference exists between the two entities. In this chapter, we shall seek to introduce the localized surface plasmon and explain what it is, how it can be created and how it supports energy transfer within nanometer-sized dimensions.

2.2. Background Information

Surface plasmons were first discovered as a result of the energy lost in an optical beam undergoing attenuated total reflection at a metal-dielectric interface. The lost energy had been coupled into surface plasmons on the surface of the metal. The plasmons arise as a result of the excitation of atoms within very small volumes on the interface between metals and dielectrics [1]. Suitably introduced optical energy perturbs electrons in the metal and displaces them slightly. However, due to the charge separation, a restoring force develops causing the quantum of excited electrons to oscillate as the surface plasmon travels along the surface of the metal.

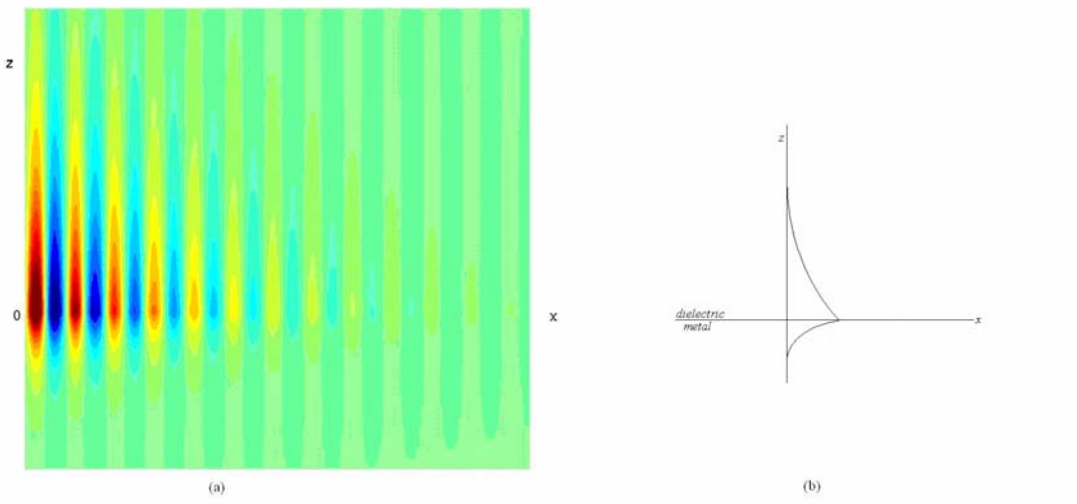

Fig.2.1a, b – Illustration of (a) calculation of a propagating surface plasmon and (b) representation of a propagating surface plasmon

An illustration of a surface plasmon in terms of the arising charges and propagation, respectively, is depicted in Fig.2.1. As shown, the strength of the surface plasmon decays exponentially in the directions perpendicular to the surface. However, the penetration depth of the plasmon into the metal and dielectric differ. These depths are on the order of the skin depth and half of the wavelength of the exciting radiation, respectively [2]. The importance of optical penetration depth in the metal will be seen in subsequent sections.

Localized surface plasmons are collective oscillations of electrons at the interface between small domains of metal and dielectric materials. In other words, localized surface plasmons can be thought of as surface plasmons that are on a non-flat surface and do not have unlimited interaction distances. The propagation of localized surface plasmons is limited to the small domains in which they exist. This results in an oscillation of the displaced electrons. A localized surface plasmon can therefore be modeled as an oscillatory dipole (Fig.2.2).

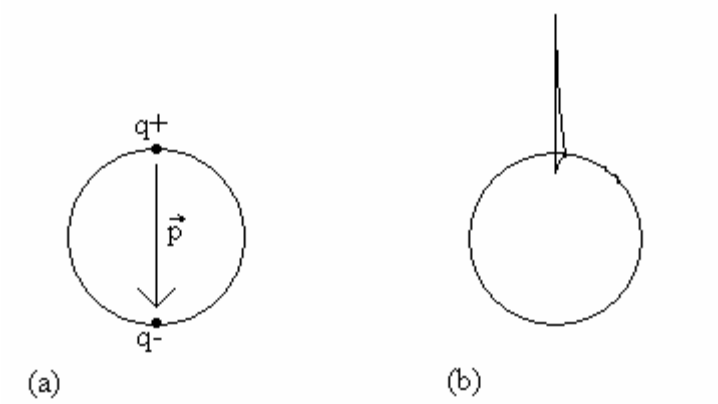

Fig.2.2 – Illustration of (a) Localized surface plasmon charges and dipole and (b) representation of a localized surface plasmon

The creation of the localized surface Plasmon is typically due to the interaction of electromagnetic energy and the atoms in these small metal domains (e.g. metallic nanoparticles). Manifestations of localized surface plasmons have been observed and include the colorful appearances of suspensions of small particles and changes in reflectivity from metals and metal-coated diffraction gratings, different from those calculated from Snell's law. In order to study surface plasmons, it is proper to understand what is needed to support them.

2.3. Conditions for Existence

In order for a localized surface plasmon to exist, certain requirements must be met. Before these conditions are mentioned, it would be appropriate to review some aspects of electromagnetic wave propagation.

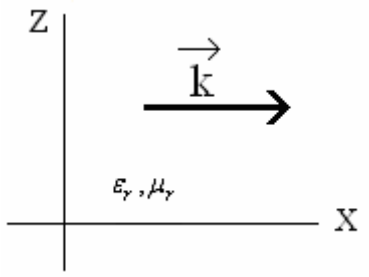

Fig.2.3 Propagation of wave in a homogenous and isotropic medium

Consider a bulk homogenous and isotropic material with dielectric constant, ε_r, and relative magnetic permeability, μ_r, with an electromagnetic wave of wave vector, k, propagating through it (Fig.2.3). Maxwell's equations give the field equations as

$$\nabla^2 \vec{E} - \mu\varepsilon \frac{\partial^2}{\partial t^2} \vec{E} = 0 \quad (2.1)$$

$$\nabla^2 \vec{H} - \mu\varepsilon \frac{\partial^2}{\partial t^2} \vec{H} = 0 \quad (2.2)$$

where $\varepsilon = \varepsilon_r\varepsilon_o$, $\mu = \mu_r\mu_o$ and ε_o and μ_o are the electrical permittivity and magnetic permeability of vacuum. One solution the these equations has a form of

$$\vec{E}(\vec{r},t) = \vec{E}_o e^{i(\vec{k}\bullet\vec{r}-\omega t)} \quad (2.3)$$

$$\vec{H}(\vec{r},t) = \vec{H}_o e^{i(\vec{k}\bullet\vec{r}-\omega t)} \quad (2.4)$$

Arising from these wave equations is the restriction that

$$k^2 = \omega^2 \mu\varepsilon, \quad (2.5)$$

which is referred to as the dispersion relation because it relates the angular outputs (or "dispersion") of waves to their respective input wavelengths. However, if we consider two different materials, a dielectric and metal, with real dielectric constants of ε_d and ε_m, respectively, that share a plane boundary as depicted in Fig.2.4, we can attempt to investigate surface plasmon propagation.

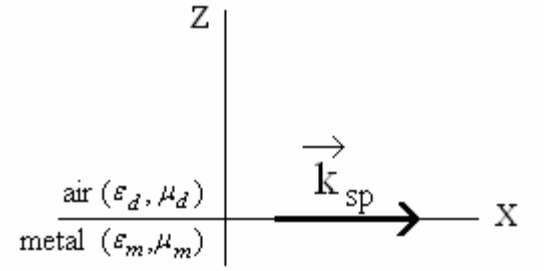

Fig.2.4 Propagation of surface Plasmon at metal-dielectric interface

Let us consider a transverse magnetic wave, i.e. a wave with the magnetic field normal to both direction of propagation and normal to the surface. Then, for the upper material (z > 0),

$$\vec{E}_1 = \begin{pmatrix} E_{x,1} \\ E_{y,1} \\ E_{z,1} \end{pmatrix} = \begin{pmatrix} E_o \\ 0 \\ ikE_o\left(k_{sp}^2 - \omega_{sp}^2\mu\varepsilon\right)^{-1/2} \end{pmatrix} e^{i\left(k_{sp}x - \omega_{sp}t\right)} e^{-\left(k_{sp}^2 - \omega_{sp}^2\mu\varepsilon\right)^{1/2} z} \qquad (2.6)$$

with $\varepsilon = \varepsilon_d\varepsilon_o$ and $\mu = \mu_d\mu_o$. For the lower material (z < 0),

$$\vec{E}_2 = \begin{pmatrix} E_{x,2} \\ E_{y,2} \\ E_{z,2} \end{pmatrix} = \begin{pmatrix} E_o \\ 0 \\ -ikE_o\left(k_{sp}^2 - \omega_{sp}^2\mu\varepsilon\right)^{-1/2} \end{pmatrix} e^{i\left(k_{sp}x - \omega_{sp}t\right)} e^{\left(k_{sp}^2 - \omega_{sp}^2\mu\varepsilon\right)^{1/2} z} \qquad (2.7)$$

with $\varepsilon = \varepsilon_m\varepsilon_o$, $\mu = \mu_m\mu_o$. In order for these equations to satisfy Maxwell's equations, certain conditions must be met. First, due to energy limitations, the amplitude of the wave cannot rise infinitely and hence

$$\left(k_{sp}^2 - \omega_{sp}^2\mu_d\mu_o\varepsilon_d\varepsilon_o\right)^{1/2} > 0 \qquad (2.8a)$$

and

$$\left(k_{sp}^2 - \omega_{sp}^2\mu_m\mu_o\varepsilon_m\varepsilon_o\right)^{1/2} > 0 \qquad (2.8b)$$

The boundary conditions, requiring that tangential continuity of $\boldsymbol{E}$ and $\boldsymbol{H}$, can be satisfied by making

$$E_{x,1} = E_{x,2} = E_o \qquad (2.9)$$

and

$$\varepsilon_d\left(k_{sp}^2 - \varepsilon_m\frac{\omega_{sp}^2}{c^2}\right)^{1/2} = -\varepsilon_m\left(k_{sp}^2 - \varepsilon_d\frac{\omega_{sp}^2}{c^2}\right)^{1/2} \qquad (2.10)$$

where is has been assumed that μ_d and μ_m are 1 for both materials (i.e. they are non-magnetic) and that $\mu_o\varepsilon_o = 1/c^2$. Equation 2.10 is satisfied only if

$$\varepsilon_m < 0 \quad (2.11)$$

Solving 2.10 for ω gives

$$\omega_{sp}^2 = \left(ck_{sp}\right)^2\left(\frac{1}{\varepsilon_d} + \frac{1}{\varepsilon_m}\right), \qquad (2.12)$$

which is the dispersion relation for a surface plasmon wave. Therefore, the three conditions necessary for surface plasmons to exist are

1. materials of different dielectric constants, ε_d and ε_m, meeting at an interface,
2. that $\varepsilon_m < 0$, and
3. that $-\varepsilon_m > \varepsilon_d$.

These conditions are satisfied by many situations simply by having a suitable metal or metal film in contact with a dielectric, say vacuum, air, or glass. Once such a setup is configured, it would be appropriate to consider how surface plasmons can be generated.

2.4.Conditions for Excitement

If the existence conditions have been met, an attempt can be made to excite surface plasmons and localized surface plasmons. The discussion here begins with a description

of the means by which surface plasmons can be excited. Then, how this relates to the excitation of localized surface plasmons will be explored.

2.4.1 Exciting Surface Plasmons

The excitation of surface plasmons can be achieved by introducing optical energy to the system in an appropriate manner. This manner requires the establishment of a match between the wave vector of the incident light and the wave vector of the surface plasmon intended to be generated in the direction of surface plasmon propagation, i.e.

$$\vec{k}_{light} = \vec{k}_{sp} \qquad (2.13)$$

The wave vector of light is obtained from Equation 2.5 while k_{sp} comes by way of a rearranged Equation 2.12. The free electron model of metals (Drude theory) can be applied to obtain the dielectric constant, ε_m of a metal. This is given by

$$\varepsilon_m = \varepsilon_m(\omega) = 1 - \left(\frac{\omega_p}{\omega}\right)^2 \qquad (2.14)$$

where ω is the incident optical frequency and ω_p is the plasmon frequency of the metal used. Substituting this into Equation 2.12 gives

$$\omega_{sp}^2 = (ck_{sp})^2 + \frac{\omega_p^2}{2} - \left[\frac{\omega_p^4}{4} + (ck_{sp})^4\right]^{1/2} \qquad (2.15)$$

for the surface plasmon and

$$\omega_{light}^2 = \frac{(ck)^2}{\mu_r \varepsilon_r} \qquad (2.16)$$

for light. Fig.2.5 shows plots of Equations 2.15 and 2.16 essentially as a function of wave vector, k, since the speed of light, c, is constant, and where it has been assumed $\mu_r = 1$, $\mu_d = 1$, and $\mu_m = 1$. This is appropriate since dielectrics and noble metals are typically non-magnetic. Also, $\varepsilon_d = 1.00$ for vacuum or air and $\varepsilon_d = 2.25$ for glass are used.

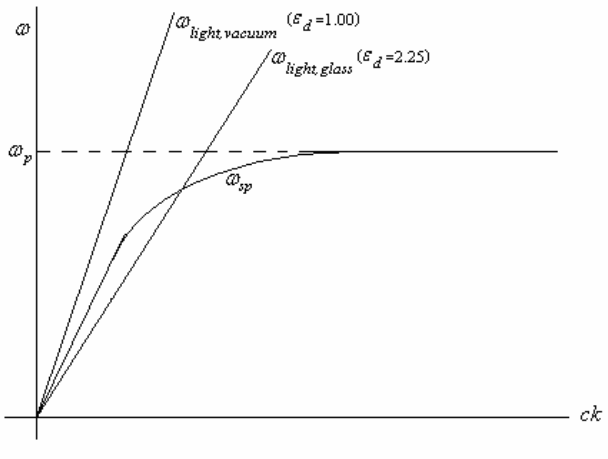

Fig.2.5 Dispersion relations of light and surface plasmons

The wave vector of light in vacuum never matches the plasmon wave vector in the optical range. Hence, surface plasmons cannot be excited directly from vacuum or air. An

optically denser dielectric, like glass for instance, is used to increase the wave vector of the light to achieve this excitation. Unfortunately, it is difficult to achieve the momentum match discussed thus far physically since Fig.2.5 considers only scalar wave number matches. A method of realizing the wave vector match was provided by Kretschmann [3] and a diagram of this method is given in Fig.2.6. Beams are assumed to be represented by their wave vectors. The incident beam refracts at the prism-air interface becoming k_i. In general, at an interface of two materials, the angle of refraction from Snell's law can be calculated as follows:

$$\theta_t = \arcsin\left(\frac{n_i}{n_r}\sin\theta_i\right) \quad (2.17)$$

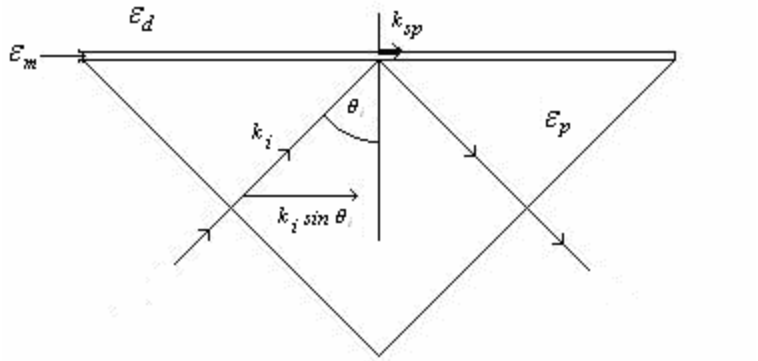

Fig.2.6 Kretschmann geometry for exciting surface plasmons on thin films

where θ_i = angle of incidence, θ_t = angle of refraction, n_i and n_r are the refractive indices of the media containing the incident and refracted rays respectively. At the prism-metal interface, $n_i = \sqrt{\varepsilon_p}$ and $n_r = \mathrm{Re}(\sqrt{\varepsilon_m})$. When the term in brackets in Equation 2.17 exceeds unity, θ_t is no longer real; physically, refraction ceases and total internal reflection (TIR) begins. Solving Equation 2.17 as applied to TIR for θ_t, we obtain

$$\cos\theta_{tir} = \pm i\sqrt{\frac{n_i^2\sin^2\theta_i}{n_r^2} - 1}\,. \quad (2.18)$$

The equation of the transmitted wave is generally of the form

$$\vec{E}_r(\vec{r},t) = \vec{E}_{o,t}e^{i\left(\vec{k}_t\bullet\vec{r}-\omega t\right)} \quad (2.19)$$

where

$$\vec{k}_t = \begin{pmatrix}\sin\theta_t\\ -\cos\theta_t\end{pmatrix} = \begin{pmatrix}\frac{n_i}{n_r}\sin\theta_i\\ -\cos\theta_t\end{pmatrix} \quad (2.20)$$

and

$$\vec{r} = \begin{pmatrix}x\\ z\end{pmatrix}. \quad (2.21)$$

Substituting Equation 2.20 and Equation 2.21 into Equation 2.19 gives

$$\vec{E}_z(\vec{r},t) = \vec{E}_{o,t} e^{i\left(x\frac{n_i}{n_r}\sin\theta_i - \omega t\right)} e^{z\sqrt{\frac{n_i^2 \sin^2\theta_i}{n_r^2} - 1}} \quad (2.22)$$

where $\boldsymbol{E_z}$ represents an evanescent wave propagating along the boundary in the plane of incidence and which varies exponentially with the distance from the boundary [4]. It is this evanescent wave, if strong enough, that couples to the metal-dielectric surface and generates surface plasmons on it. This happens at some angle, $\theta_i = \theta_{sp}$, where the wave vector match is

$$k_{light,vacuum}\sqrt{\varepsilon_p}\sin\theta_{sp} = k_{sp}. \quad (2.23)$$

The evanescent wave loses strength rapidly in the z direction and, hence, its penetration depth poses a limit on how far away from the prism surface plasmons can be created. In fact, the distances are so small that almost always metallic films must be used in place of bulk metal for this arrangement of prism, metal and dielectric. The surface plasmons generated propagate along the surface and lose their strengths in various ways which include lattice interactions and far field radiation. While not exactly localized surface plasmons, this analysis for surface plasmons is related significantly to them.

2.4.2 Exciting Localized Surface Plasmons

Our discussion, so far, has centered on surface plasmons. Localized surface plasmons can be considered as a superset of surface plasmons. Alternatively, surface plasmons may be thought of as localized surface plasmons on surfaces whose radii are at infinity. The corollary of that statement implies that localized surface plasmons are generated by similar means that satisfy the condition in Equation 2.13. The domain dimensions often make meeting this condition possible with much simpler means. However, the sizes of metal particles on which these plasmons can be excited give rise to interesting electronic effects. Similar processes take place when light impinges on these particles; at the right incident angles, tunneling across the particle occurs and generates surface plasmons on the particle. Fig.2.7 illustrates this which often happens when the particles are illuminated in a solution where the solvent is a nonconductive dielectric. The tunneling distance is often less than optical penetration depth, which is on the order of several tens of nanometers.

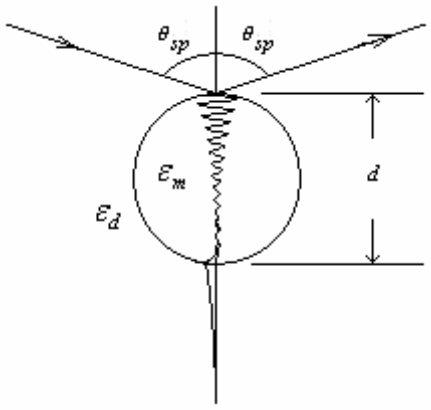

Fig.2.7 Exciting localized surface plasmons in an unbound nanoparticle

The surface plasmon angle is easily achieved when random scattering occurs between many particles, especially so for spherical particles since some wave vectors will always be at the surface plasmon angle. For nanoparticles that have been localized, geometries similar to those described for surface plasmons can be used. Consider a spherical metallic particle on a dielectric at a point of incidence at which TIR is taking place (Fig.2.8a). This is a special case of the Kreschmann method described earlier. The evanescent wave couples into the metallic nanoparticle, tunnels across and excites a localized surface plasmon in the nanoparticle. Again the optical penetration depth impacts how far the evanescent wave tunnels and, therefore, affects the number of electrons that get excited.

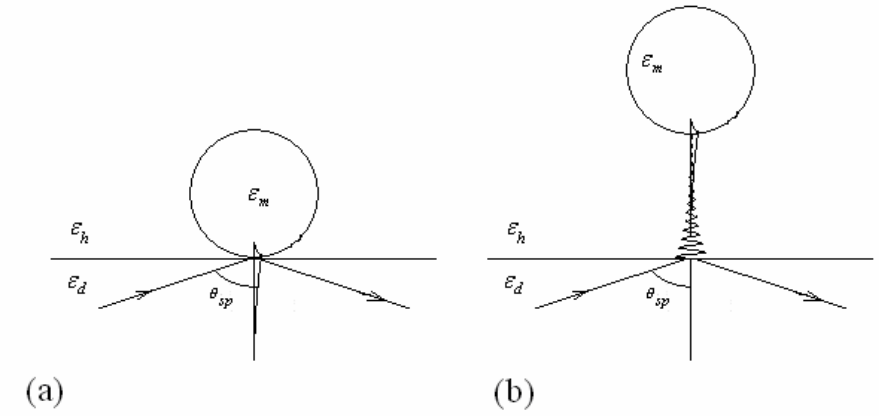

Fig.2.8 Exciting localized surface plasmons in bound nanoparticles by the (a) Kretschmann and (b) Otto geometries

Another possible geometry, attributed to Otto [5], is depicted in Fig.2.8b. Here, the nanoparticle is some distance away from the point of incidence where total internal reflection occurs. The evanescent wave tunnels through the dielectric between the prism and the particle and excites a localized surface plasmon in the particle upon reaching it. There are other ways of exciting surface plasmons but these are the ones of main interest in this project.

2.5. Nature of Charges on Particle Arising from Surface Plasmon Excitation

When localized surface plasmons are excited in metallic nanoparticles, strong resonances are observed. These arise from the displacement of conduction electrons [6]. These separated charges form a dipole, which can be represented by ***p***. This displacement is not done once; the displaced electrons set up a dipolar restoring force, which leads to an oscillation of electrons in the nanoparticle. The oscillations get weaker with time as they are damped out. Fig.2.9 shows this along with the orientation of the polarization vector with time.

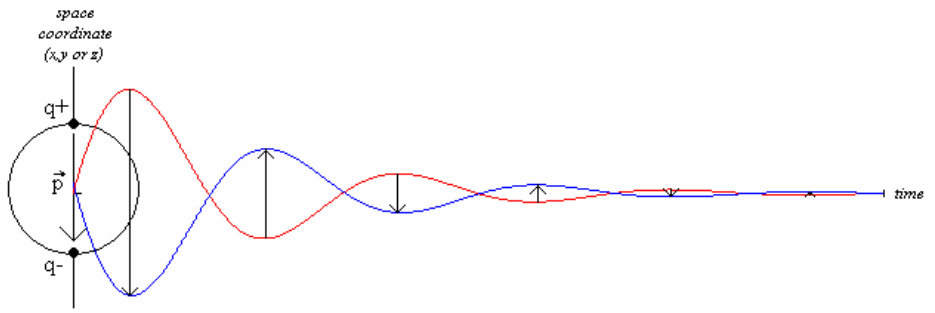

Fig.2.9 Localized surface plasmon polarization vector over time

There is a strong nanoparticle size dependency on the quantum of electrons that are displaced in the particle. For gold, virtually all the conduction electrons in nanoparticles with diameters less than 25nm are excited. This applies to other small particles [7] and is called the intrinsic size effect [8]. As the particles get larger, the total number of electrons in the particle that are excited drops. The incident radiation, instead of causing bulk excitation of the electrons in the particle, excites localized areas on the particle. These multi-polar electronic oscillations, also categorized as the extrinsic size effect [8], arise and the surface plasmon resonance shifts and decreases.

2.6. Nanoparticle Field Emissions and Enhanced Fields

The dipole created as a result of localized surface plasmon excitation exists as an oscillatory dipole whose strength decreases over time. Mie [9] developed a theory for fields interacting with nanoparticles. In the quasi-static approximation, which assumes the field is spatially static, Okamoto [10] has shown that the induced scattering field outside an arbitrary small metallic sphere is identical to the field of an oscillating dipole of moment, ***p*** at the center of the metal sphere and given by

$$\vec{p} = \varepsilon_m \alpha \vec{E}_o \qquad (2.24)$$

with

$$\alpha = 4\pi r_1^3 \left(\frac{\varepsilon_d - \varepsilon_m}{\varepsilon_d + 2\varepsilon_m} \right) \quad (2.25)$$

where r_1 is the radius of the particle and ε_d and ε_m are the dielectric constants of the host and metal, respectively. However, the dipole retains the time dependency, $exp(i\omega t)$, of the external field that created it, $\boldsymbol{E_0}$. Oscillating dipoles produce electric and magnetic fields given by [11] as

$$\vec{E} = \frac{1}{4\pi\varepsilon_2} \left(-\frac{\vec{p}(t_o)}{r^3} + \frac{3\vec{r}\left[\vec{r} \bullet \vec{p}(t_o)\right]}{r^5} + \frac{ik\vec{p}(t_o)}{r^2} - \frac{3ik\vec{r}\left[\vec{r} \bullet \vec{p}(t_o)\right]}{r^4} - \frac{k^2}{r^3}\vec{r} \times \left[\vec{r} \times \vec{p}(t_o)\right] \right)$$

(2.26)

$$\vec{H} = -\frac{i\omega}{4\pi} \left(\frac{1}{r^2} - \frac{ik}{r} \right) \vec{r} \times \vec{p}(t_o) \quad (2.27)$$

where $t_o = t - kr/\omega$ and k is the wave vector in the dielectric. If we separate the electric fields [12] such that

$$\vec{E}_P = \vec{E}_F + \vec{E}_M + \vec{E}_R, \quad (2.28)$$

then

$$\vec{E}_F = \frac{1}{4\pi\varepsilon_2}\left(-\frac{\vec{p}(t_o)}{r^3} + \frac{3\vec{r}\left[\vec{r} \bullet \vec{p}(t_o)\right]}{r^5}\right) \quad (2.29)$$

$$\vec{E}_M = \frac{1}{4\pi\varepsilon_2}\left(\frac{ik\vec{p}(t_o)}{r^2} - \frac{3ik\vec{r}\left[\vec{r} \bullet \vec{p}(t_o)\right]}{r^4}\right) \quad (2.30)$$

$$\vec{E}_R = \frac{1}{4\pi\varepsilon_2}\left(-\frac{k^2}{r^3}\vec{r} \times \left[\vec{r} \times \vec{p}(t_o)\right]\right) \quad (2.31)$$

where $\boldsymbol{E_F}$ is the static field [10] or Förster field [12], $\boldsymbol{E_M}$ is the induction field [10] and $\boldsymbol{E_R}$ is the radiation field [10,12]. The static field dominates when the radius of the particle is much smaller than the wavelength of the incident radiation while the radiation field dominates when the relationship is reversed [12]. Of the three fields, only the radiation field propagates to infinity [10]. Given the dimensions of the particles used in this project (~20nm in diameter), the static field is most dominant. This forms the bulk of the near field of the localized surface plasmon, along with the induction field. Compared to other scenarios of electric fields radiated by structures of various dimensions, the electric fields generated by these particles are exceptionally large. This is largely due to the (r^{-3}) dependency of the static field and the fact that the relevant lengths of r on this scale are indeed very small.

Several uses have been found for such enhanced fields and include sensing the propagation of energy along plasmonic waveguides [13, 14, 6]. Fluorescent dyes of suitable frequency response and physical placement with respect to the metal nanoparticle are used to convert the plasmonic near field into electromagnetic radiation that can be collected and observed in the far field. Also, plasmonic waveguide operation depends on the interaction of the near field and any improvements to the magnitude and coupling ability of this field improves waveguide performance.

2.7. Effects of Nanoparticle Size and Shape

Section 2.4 mentioned briefly how nanoparticle size affects the displacement of electrons as they relate to localized surface plasmon excitation. There are a few more phenomena associated with the size and shape of particles, which will not be described in this text as they have minimal impact on the performance of plasmonic waveguides.

2.7.1 Effects of Size

The size of a particle relates directly to its extinction ratio, which is a measure of the transmission and absorption of a particle. A common equation is given by [6] as

$$\sigma_{ext} = 9\frac{\omega}{c}\varepsilon_d^{\frac{3}{2}}V_o\frac{\varepsilon_2}{\left[\varepsilon_1 + 2\varepsilon_d\right]^2 + \varepsilon_2^2} \quad (2.32)$$

where σ_{ext} = extinction ratio and V_o = volume of particle. The size of a particle, therefore, has a direct impact on the amplitude of the localized surface plasmon, or how

well the electrons in the particle resonate at the material's resonant frequency. The electrons in larger particles tend to resonate less as compared to those of smaller particles for several reasons. Some of these reasons include the loss of the en masse displacement of electrons in the nanoparticle and the sheer bulk of a larger particle, which dampens the tunneling across it. This is related to the extrinsic size effect mentioned earlier. Red shifts also occur with particles of increasing size.

2.7.2 Effects of Shape

Shape also affects its resonance properties. When particles have nonsymmetrical shapes, the electrons begin to demonstrate resonances associated with each of the dimensions. For instance, while a spherical nanoparticle may have a single resonant frequency related to its singular dimension, i.e. its radius, an ellipsoidal particle may have two or three resonance frequencies related it to its two or three axes [6]. These differences arise from different orientations and magnitudes of the dipoles on the ellipsoidal particles and results in distinct resonance frequencies for each dimension [6, 15]. In colloidal chemistry, some amount of control over particle shape is available and this can be used to fashion out relevant properties and phenomena.

2.8. References

[1] Zayats, Smolyaninov, "Near field Photonics: surface plasmon polaritons and localized surface plasmons", J. Opt. A. Pure Appl. Opt. 5 (2003) S16-S50

[2] W.L. Barnes, A. Dereux, and T.W. Ebbesen, "Surface plasmon subwavelength optics", Nature Vol.424, 824-830, August 2003

[3] Kretschmann, E. Optical Communication, 1972, 6, 185

[4] Born and Wolf, "Principles of Optics", 5th Ed., 1975

[5] A. Otto, Z. Phys 216, 398, 1968

[6] S.A. Maier, P.G. Kik, H.A. Atwater, S. Meltzer, A.A.G. Requicha, B.E. Koel, "Observation of coupled plasmon-polariton modes of plasmon waveguides for electromagnetic energy transport below the diffraction limit", Proceedings of SPIE, Vol. 4810

[7] K.L. Kelly, E. Coronado, L.L. Zhao, and G.C. Schatz, "The Optical Properties of Metal Nanoparticles: The Influence of Size, Shape, and Dielectric Environment", J. Phys. Chem. B 107, 668-677, 2003

[8] S. Link, and M.A. El-Sayed, "Optical Properties and Ultrafast Dynamics of Metallic Nanocrystals", Annu. Rev. Phys. Chem. 54, 331-366, 2003

[9] G. Mie, Beitrage zur Optik truber Medien, speziell kolloidaler Metallosungen. Ann Phys. (Leipzig) 25, 377-445 (1908)

[10] Takayuki Okamoto, "Near field spectral analysis of metallic beads", Appl. Phys. 81, 97-122, (2001)

[11] J.A. Stratton, Electromagnetic Theory (McGraw-Hill, New York 1941)

[12] M.L. Brongersma, J.W. Hartman, H.A. Atwater, "Electromagnetic energy transfer and switching in nanoparticle chain arrays below the diffraction limit", Phys Rev B, Vol. 62, No. 24, December 2000

[13] J.R.Krenn, H. Ditlbacher, G. Schider, A. Hohenau, A. Leitner, F.R. Aussenegg, "Surface Plasmon micro- and nano-optics", Journal of Microscopy, Vol. 209, Pt.3 March 2003, pg167-172
[14] S.A. Maier, P.G. Kik, H.A. Atwater, S. Meltzer, E. Harel, B. Koel, A.A.G. Requicha, "Local detection of electromagnetic energy transmitted below the diffraction limit in metallic nanoparticle plasmon waveguides", Nature Materials, Vol. 2, April 2003
[15] S.A. Maier, M.L. Brongersma, P.G. Kik, S. Meltzer, A.A.G. Requicha, H.A. Atwater, "Plasmonics – A route to nanoscale optical devices," Adv Mat 2001, 13, No.19, October 2

Chapter 3

Plasmonic Arrays

3.1 Introduction

Having introduced the mechanism by which nanoparticles support localized surface plasmons, this chapter introduces how an array of such nanoparticles, by way of excited localized surface plasmons and near field interactions, can guide these plasmonic interactions over increased distances. In addition, the mechanics of the plasmonic array are discussed – energy transfer and effects of particle size and spacing among other things. The chapter rounds up with some discussion about plasmonic waveguide losses.

3.2 Near field Energy Transfer

In Chapter 2, the large electric near field of an excited localized surface plasmon in a metallic nanoparticle was discussed. It is this field which is largely responsible for plasmonic waveguiding action. It provides the means for coupling energy from one nanoparticle to the next in a linear chain, forming a plasmonic waveguide.

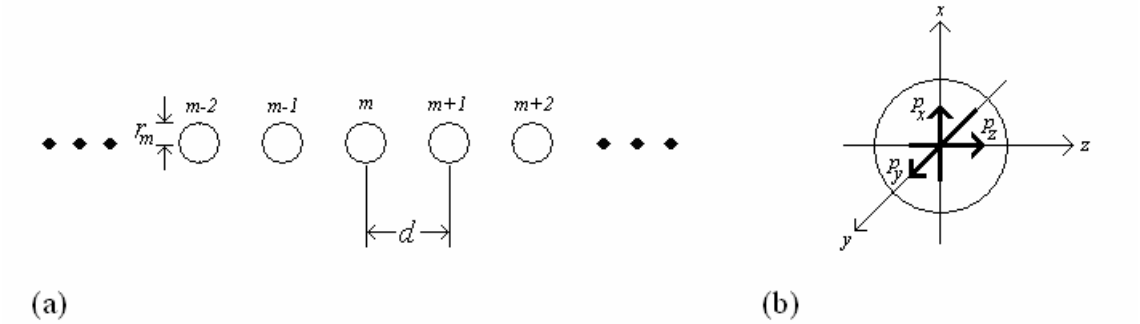

Fig.3.1 Illustration of (a) plasmonic waveguide, and (b) dipoles on an excited metal nanoparticle

Consider a row of particles (Fig.3.1a), each with radius r_m and separation d between centers. The mth particle in the chain is assumed to have been excited by a suitable means so that an oscillating dipole, $\boldsymbol{p}$, can be assumed to exist in it. The electric field radiated by this dipole has been given by Equation 2.26. At the nearest neighbors, only the electric near field matters and can be obtained from Equation 2.28. This field depends on the direction of the dipole oscillation (shown in Fig.3.1b). For an oscillating dipole $\boldsymbol{p}$ the electric field is given by [1] as

$$E_{i.m} = \frac{\gamma_i p_{i,m}(t)}{4\pi\varepsilon_o n^2 d^3} \qquad (3.1)$$

where γ_i = is a polarization dependent constant with γ_L = -2, γ_T = 1 and L and T represent longitudinal (p_z) and transverse (p_x or p_y) dipoles, respectively, and n is the refractive

index of the dielectric surrounding the particle. There is also a sign change, which is an arbitrary difference especially for time harmonic fields. Nearest neighbor interactions have been considered due to the rapidity with which the near field loses strength and, hence, the almost insignificant contributions made by particles further away. However, it is often difficult to excite a single particle in a row as described. If several particles are excited in unison, as is more often the case, the same equations apply for each particle and its nearest neighbors. For a chain of Hertzian dipoles [2], with $p = Qr_p$, where Q is charge on particle and r_p is the distance from equilibrium in the i direction at point m in the chain, the dipole motion is given in [1] as

$$\frac{\partial^2}{\partial t^2} p_{i,m} = -\omega_o^2 p_{i,m} - \Gamma_l \frac{\partial}{\partial t} p_{i,m} + \frac{\Gamma_R}{\omega_o^2} \frac{\partial^3}{\partial t^3} p_{i,m} - \gamma_i \omega_1^2 \left(p_{i,m-1} + p_{i,m+1} \right) \quad (3.2)$$

where accordingly the first term represents the dipole eigenmotion at ω_o, the angular velocity of the incident radiation; the middle two terms represent losses to damping and the far field, and the last term represents the electrodynamic nearest neighbor interactions. The term, ω_1, is a coupling strength parameter that represents nearest neighbor interactions. It is from the last term that propagation solutions arise. The coupling strength constant of the chain depends on particle size and particle separation which are represented in ω_1, given as

$$\omega_1^2 = \frac{N_e q^2}{4\pi m_{o,eff} \varepsilon_o n^2 d^3} \quad (3.3)$$

where N_e = the number of electrons oscillating, q = electron charge and $m_{o,eff}$ = optical effective electron mass. This applies well in the intrinsic size effect regime where all electrons in the particle are assumed to be involved in the dipole oscillation. The closer the orders of ω_1 and ω_o are, the higher the coupling strength. Propagation solutions are of the form

$$p_{i,m=} P_{i,o} \exp\left[-\alpha m d + i\left(\omega t \pm k m d \right) \right] \quad (3.4)$$

where $(\omega t - kmd)$ applies when the phase and group velocities are parallel, and $(\omega t + kmd)$ applies when the phase and group velocities are anti-parallel. The value of $P_{i,o}$ determines the dipole moment at $m = 0$ in the polarization direction i [1]. The damping of the plasmon wave per unit length is given by the attenuation factor α. The plasmon wave angular frequency and wave vector are given by ω and k, respectively. The angular frequency is given by

$$\omega^2 = \omega_o^2 + 2\gamma_i \omega_1^2 \cos(kd), \quad (3.5)$$

which is the dispersion relationship for plasmon waves on a plasmonic waveguide. Applying the standard definition of group velocity gives

$$\upsilon_{g,i} = \gamma_i \omega_1^2 d \frac{\sin(kd)}{\omega} \quad (3.6)$$

The attenuation factor is given by

$$\alpha = \frac{\Gamma_l + \frac{\omega^2}{\omega_o^2} \Gamma_R}{2\upsilon_g} \quad (3.7)$$

and

$$\Gamma_l = \frac{\upsilon_F}{\lambda_B} + \frac{C\upsilon_F}{R} \qquad (3.8)$$

$$\Gamma_R = \omega_o^2 \tau \qquad (3.9)$$

and

$$\tau = \frac{2q^2}{3mc^3}. \qquad (3.10)$$

Γ_l is the electronic relaxation frequency due to interactions with phonons, electrons, lattice defects and impurities. It depends on the electron mean free path in the bulk material, λ_B, the Fermi velocity, v_F, and a constant, C, which is approximately 1. Γ_R is the relaxation frequency due to radiation into the far field [1].

3.3 Effects of Inter-particle Spacing

The spacing between particles has a significant effect on the wave guiding characteristics of plasmonic waveguides. As the inter-particle spacing increases the electric field seen by adjacent particles drops, which leads to a reduction in coupling strength. For instance, a doubling of the inter-particle spacing in Fig.3.1a leads to the coupling strength dropping to an eighth of its original value. In such a system, more energy is lost to the damping mechanisms than is transmitted along with plasmonic waveguide. Some amount of control over inter-particle spacing is available in self-assembly processes and more of this will be discussed in subsequent chapters.

3.4 Effect of Particle Size Distribution

Particle size variation is an important issue since nanoparticles synthesized by colloidal means often display this. The variations in size lead to variations in the magnitudes of the induced dipoles, which lead to variations in the fields that are radiated along a plasmonic waveguide. Slight variations in the dispersion along the waveguide arise and may lead to interesting effects, which may include a non-uniform distribution of the plasmon waves and different modes along the waveguide. Most of the affected parameters would have to be discussed statistically in order for meaningful data and discussions to be obtained. It would be most ideal if means were found to reduce or eliminate the size distributions that could lead to such difficulties.

3.5 Losses Arising

The primary losses that arise are due to damping. Energy loss to phonons, electrons, lattices and impurities and losses due to coupling to the far field are the two major mechanisms. These are inherent constraints that are ever-present and limiting. Losses on the order of 3dB/15nm [3] and 6dB/200nm [4] have been reported.

3.6 References

[1] M.L Brongersma, J.W. Hartman, H.A. Atwater, “Electromagnetic energy transfer and switching in nanoparticle chain arrays below the diffraction limit”, Phys Rev B, Vol. 62, No. 24, December 2000
[2] Walter Greiner, Classical Electrodynamics, Springer-Verlag, New York, 1996
[3] S.A. Maier, P.G. Kik, H.A. Atwater, S. Meltzer, A.A.G. Requicha, B.E. Koel, “Observation of coupled plasmon-polariton modes of plasmon waveguides for electromagnetic energy transport below the diffraction limit”, Proceedings of SPIE, Vol. 4810
[4] S.A. Maier, P.G. Kik, M.L. Brongersma, “Energy transport in metal nanoparticle plasmon waveguides”, Mat. Res. Soc. Symp. Proc. Vol. 777, T7.1.1

Chapter 4

Nanoparticles in Thin Films

4.1 Introduction

So far, the theory associated with surface plasmons and plasmonic waveguides has been described. Colloidal nanoparticles were used for the structures that were fabricated in this project. This chapter begins with an overview of how these nanoparticles are made. It goes on further to discuss how these particles can be self-assembled on substrates from which waveguides may be etched. The experimental methods are presented in Chapter 5 and discussed in the following chapter.

4.2 Colloidal Nanoparticles

Gold colloids have been explored well explored [1]. The definition of a colloid is varied but is generally understood to include a state of subdivision in which the particles, droplets or bubbles dispersed in another phase have at least one dimension between approximately 1nm and 1000nm [2]. Nanoparticle colloids typically have particles with nanometer dimensions ranging from nanometers to tens or a few hundreds of nanometers.

For this project, gold nanoparticles were synthesized in an aqueous solution using a well studied colloidal synthesis process [3]. These solutions were produced by the co-precipitation of gold from a gold salt ($HAuCl_4$) solution. A surfactant (sodium citrate) was used to inhibit the particles from sticking together and forming a solid mass, a process known as aggregation or agglomeration, which would have defeated the intended purpose of the experiment. Varying concentrations and volumes of the reactants lead to different properties in the nanoparticles produced. This shall be discussed further later.

4.3 Colloidal Nanoparticle Alignment Methods

In order to produce waveguides, suitable means of assembling the nanoparticles from colloidal solution onto substrates from which waveguiding structures may be produced is necessary. There are a few options that have been developed to date, but so far most have focused on the individual placement of nanoparticles [4]. For instance, methods using electron beam lithography, atomic force microscopy or near field scanning optical microscopy are able to place individual particles precisely but these methods do not lend themselves to inexpensive and quick fabrication or manufacturing [5,6]. The overriding intent of this work is to achieve such manufacturability and cheapness, hence the interest in bulk assembly methods. Two methods that were considered were self assembly by ionic self-assembled monolayers (ISAMs), which is described in Section 4.3.1, and by diblock copolymers, which is described in Section 4.3.2.

4.3.1 Ionic Self-Assembled Monolayers

ISAMs are ionically self-assembled monolayers. The earliest work in this area was undertaken by Iler [7], but other researchers, such as Decker [8], have taken the process to new heights. It is indeed possible to create layers of molecules on a prepared surface by using appropriate polyelectrolytes and conditions. The substances that self-assemble are polyelectrolytes and are typically water-soluble. Polycationic polyelectrolytes are positively charged while polyanionic polyelectrolytes retain a negative charge. The ISAM self-assembly process can be started, for instance, with a surface of negative charge. This charged surface is immersed in a polycationic electrolyte and its molecules attach themselves uniformly to the negative charge. The attachment is virtually complete in minutes; McAloney [9] has suggested that the initial attachment might take place within the first 10 seconds of immersion. Excess electrolyte molecules are removed by rinsing with water and the process is repeated with a polyanionic electrolyte, which also self-assembles on the polycationic layer. The result so far is an A-B type layer of two polyelectrolytes. Several of these layers can be built upon each other to create a particular structure. In addition, several different polyelectrolytes can be used and the process lends itself to forming various structures including quadlayers of the form A-B-A-C. Such structures can be used to increase spacing in a given direction in the device.

If a gold colloid can be made to act like a polyelectrolyte then, by this process, these nanoparticles can be embedded in the layer. This can be done by altering the surface of the particles in such a manner that they become either positively or negatively charged, which give polycationic or polyanionic electrolytes, respectively. Two common methods of achieving this have been by using an alkyl thiol molecule functionalized with either an amine ($-NH_2$) group or a carboxy (-COOH) group [10]. The thiol group (-SH) has a strong reactivity with gold and therefore attaches to the gold nanoparticle. The hydrolyzed functional end, either amine ($-NH_3^+$) or carboxy ($-COO^-$), stretches away from the particle due to electrostatic interactions, and binds to either polyanions or polycations, respectively, in the ISAM process (Fig.4.1).

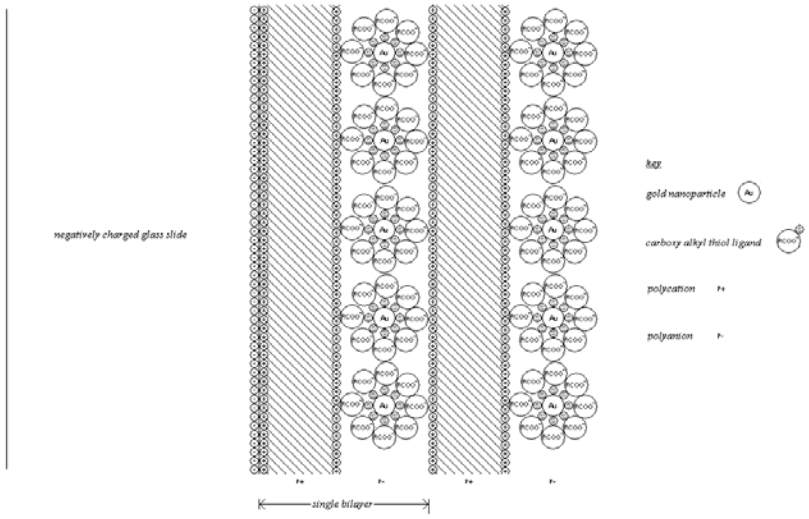

Fig.4.1 Illustration of ISAM layers with a polycation and carboxy alkyl thiol-capped gold nanoparticles as polyanion

A single bilayer can be built by dipping a negatively charged glass substrate into a polycation and then into a solution of gold nanoparticles capped with a carboxy alkyl thiol, which acts as a polyanion due to the $-COO^-$ group. If the density of nanoparticles in a single layer is high enough and shows near field interactions then plasmonic waveguiding may be possible. Also, several layers of these polyelectrolyte films can be made to produce alternating layers that contain nanoparticles. These films can then be etched appropriately to pattern waveguides in an appropriate direction on the film.

4.3.2 DiBlock Coploymers

Diblock copolymers are composed of two different polymer chains attached at their ends [11]. They are typically made by complicated polymerization methods, which are beyond the scope of this project [10,12,13]. Under certain conditions, the constituent polymers retain their individual properties and these differences can be used for patterning. For example, a diblock copolymer can be dissolved in an appropriate solvent and spin coated on a substrate. Upon drying, and depending on the solubility of the individual constituent polymers in the common solvent, the polymers may separate into two different phase distributions. For instance, a diblock copolymer composed of a 70:30 mixture between polymethyl methylacrylate (PMMA) and polystyrene (PS) and spun coated on a surface below a certain thickness, the intrinsic polymer-length scale, shows a separation between PMMA and PS domains upon annealing [14,15]. Depending on the copolymer properties, the PMMA domains may form hexagonal close packed structures in the PS matrix [14]. Either of these domains can be made to contain nanoparticles via the use of suitable chemical reactions between functionalized nanoparticles and the appropriate polymer half of the diblock copolymer. For instance, gold nanoparticles can be preferentially located in the PS domains of a PS-PMMA phase separation by coating the gold nanoparticles with polystyrene-thiol (PS-SH) polymer [16]. Alternatively, gold nanoparticles, which react with poly-2-vinly pyridine (P2VP), can be preferentially placed in the P2VP parts of the PS-b-P2VP block copolymer. Spin coating the resulting polymer-nanoparticle solution would show gold nanoparticles in the P2VP domains. Patterning can be achieved by the removal of the other domain by an appropriate means, usually a selective etch or solvent [15]. For example, acetic acid has been used to remove PMMA domains [17]. This would leave nanoparticles assembled on a two-dimensional surface available for etching into waveguides.

4.4 Exciting Plasmonic Waveguides

Three means of exciting plasmonic waveguides are often used. These are the Kretschmann and Otto geometries, along with far field excitation. These are described in the following three subsections.

4.4.1 Kretschmann Geometry

This method is similar to the method as described in Chapter 2 for exciting surface plasmons on a metallic film. It is also known as the prism-metal-vacuum method. A

diagram of this method as applied to exciting plasmon waveguides is given in Fig.4.2. Once the wave vector match has been made, the evanescent wave due to total internal reflection radiates away from the prism-metal interface into the metal film. At the metal-air (or dielectric) interface, the tunneling evanescent wave excites a surface plasmon. However, the nanoparticles are placed sufficiently close enough to the metal film for the surface plasmon at the metal-dielectric interface to excite localized surface plasmons in them. Once this is achieved the energy transfer continues between nanoparticles. This method can also lend itself to easy visualization of the energy propagating along the nanoparticle arrangement. If the dielectric-metal film boundary is sufficiently rough due to the thin film deposition process, the interaction between the localized surface plasmons in the particles and the defects in the metallic film will lead to a release of optical energy that can be seen in the far field.

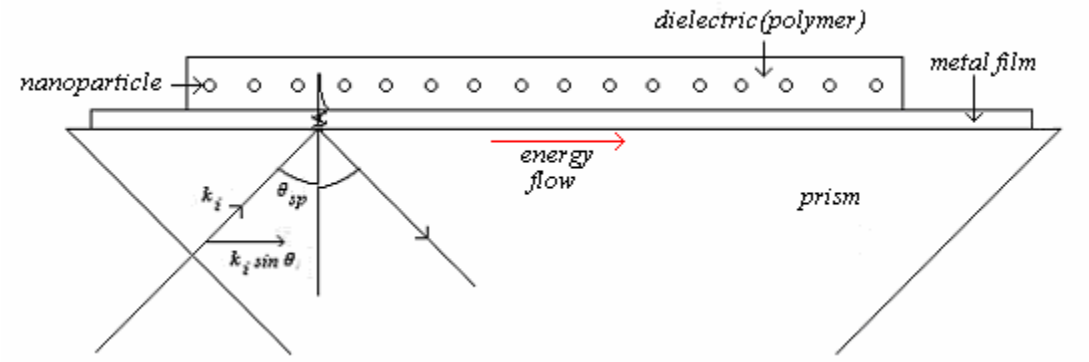

Fig.4.2 Kretschmann Geometry for exciting plasmonic waveguides

One difficulty of this method is that a thin film must be used. Once a metal film is attached to a given prism, it remains on the prism and other films cannot be used unless the original metallic film is removed. There is a method, the Otto geometry, that overcomes this limitation.

4.4.2 Otto Geometry

This geometry is also known as the prism-vacuum-metal geometry, shown in Fig.4.3. The "vacuum" region contains either a vacuum or a suitable dielectric. It is in this region that the plasmonic waveguide remains. Again, total internal reflection takes place in the prism, producing an evanescent wave that tunnels through the vacuum region and produces surface plasmons on the metal surface. It may also produce localized surface plasmons directly on the nanoparticles. Furthermore, the surface plasmons created on the metal surface interact with the nanoparticles and produce localized surface plasmons on them.

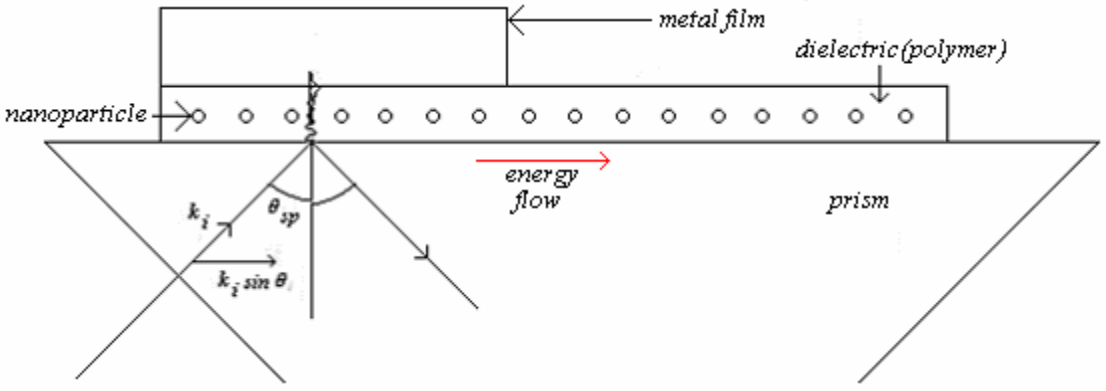

Fig.4.3 Otto Geometry for exciting plasmonic waveguides

The metal in this case need not be a thin film as there is no need for the evanescent wave to tunnel through the metal completely. Also, the metal can be changed very rapidly to compare how well different films support the waveguides. Unfortunately, direct visualization of the surface plasmon excitation and propagation is difficult. Often, the waveguide is observed by looking at the light coming off the prism-vacuum interface through the prism.

4.4.3 Far field Excitation

Plasmonic waveguides can be excited by far field light. To achieve this, illustrated in Fig. 4.4a, a tight beam of light is focused on the particles causing localized surface plasmons to be generated in them directly [18].

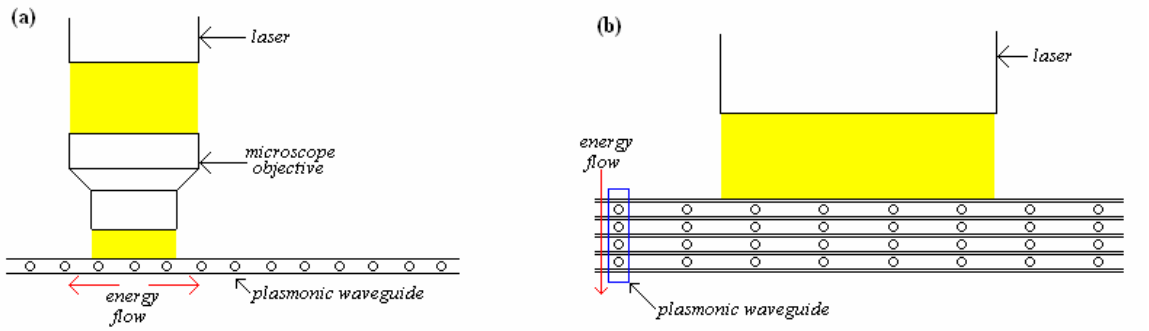

Fig.4.4 Far field excitation of plasmonic waveguides illustrating (a) intra-film excitation, and (b) inter-film excitation. Waveguide sizes are exaggerated.

These plasmons set up near fields in their immediate vicinities and particles in close proximity are excited. However, given the distances that the optical energy propagates, it is essential that a beam of very small diameter is used in order that the propagating energy can be observed beyond the beam. Laser radiation is typically focused by a high magnification microscope objective to achieve this. However, if the particles are not in close proximity with each other, near field interactions are markedly reduced and each particle responds individually. If several layers like this are placed very close to each other, while intra-film particle interactions may be insignificant, inter-film particle interactions may be significant, depending on the thickness of the separating layer. With self-assembly, these distances can be small and if several layers are stacked, some

plasmonic waveguiding action due to the inter-film interaction can be observed as the number of layers increases (Fig.4.4(b)). This is due to the interaction of particle near fields across layers.

4.5 Monitoring Energy Propagation

For characterization and indeed for device operation it is important to have a means of measuring observing energy flow along the nanoparticle assembly. Methods of introducing energy into the waveguide have already been discussed; in current literature the main methods are detecting the near fields by using fluorescent dyes [17,18] that react to the near fields or by using NSOM tips or rough metallic thin film surfaces that can detect and show, respectively, the electric near field.

When fluorescent dyes are used, it is important to place the dye molecules approximately 30nm away from the nanoparticles so as to balance the typical photoluminescence quenching effects of the nanoparticles as opposed to their ability to couple enough of the electric near field to far field optical radiation. These dyes are typically spin-coated onto the surface of the waveguide after a spacing layer is deposited. For direct observation via interactions between localized surface plasmons and rough metallic thin films, a metallic film that is placed close but not in contact with the particles acts as a rough surface. The surface defects in this film become points at which the electric near field is perturbed and far field light is emitted. The intensities over distances, bends and other such arrangements can be quantitatively obtained.

4.6 References

[1] M.A. Hayat, “Colloidal Gold: Principles, Methods and Applications”, Academic Press, Inc, Vol. 1-3, 1989,1991

[2] L.L Schramm, “Dictionary of Colloid and Interface Science”, Wiley & Sons, 2001

[3] J. Turkevitch, P.C. Stevenson, J. Hillier, “Nucleation and growth process in the synthesis of colloidal gold”, Discussions of the Faraday Society, 11, 55, 1951

[4] S.A. Maier, M.L. Brongersma, P.G. Kik, S. Meltzer, A.A.G. Requicha, H.A. Atwater, “Plasmonics – A route to nanoscale optical devices,” Adv Mat 2001, 13, No.19, October 2

[5] S.A. Maier, P.G. Kik, H.A. Atwater, S. Meltzer, A.A.G. Requicha, B.E. Koel, “Observation of coupled plasmon-polariton modes of plasmon waveguides for electromagnetic energy transport below the diffraction limit”, Proceedings of SPIE, Vol. 4810

[6] S.A. Maier, P.G. Kik, H.A. Atwater, S. Meltzer, E. Harel, B. Koel, A.A.G. Requicha, “Local detection of electromagnetic energy transmitted below the diffraction limit in metallic nanoparticle plasmon waveguides”, Nature Materials, Vol. 2, April 2003

[7] R. K. Iler, “Multilayers of colloidal particles”, J. Colloidal Interface Sci., 21, 569-594, 1966

[8] Decker, “Buildup of ultrathin multilayer films by self-assembly process: II. Consecutive adsorption of anionic and cationic bipolar amphiphiles and

polyelectrolytes on charged surfaces", Ber. Bunsen-Ges. Phys. Chem., 95, 1430-1434, 1991
[9] R.A. McAloney and M.C. Goh, "In Situ Investigations of Polyelectrolyte Film Formation by Second Harmonic Generation", J. Phys. Chem. B, 103, 10729-10732, 1999
[10] A. Kumar, A.B. Mandale, M. Sastry, "Sequential Electrostatic Assembly of Amine-Derivatized Gold and Carboxylic Acid-Derivatized Silver Colloidal Particles on Glass Substrates", Langmuir 2000, 16, 6921-6926
[11] I.W. Hamley, "Introduction to Block Copolymers", Developments in Block Copolymer Science and Technology, John Wiley & Sons, Ltd, 2004
[12] Folkes, "Processing, Structure and Properties of Block Copolymers",Elsevier Applied Science, 1985
[13] Noshay, McGrath, "Block Copolymers – Overview and Critical Survey", Acedemic Press, 1977
[14] Black and Bezencenet, "Nanometer-Scale Pattern Registration and Alignment by Directed Copolymer Self-Assembly", IEEE Trans. Nanotechnology, Vol.3, No.3, September 2004
[15] K.W. Guarini, C.T. Black, Y. Zhang, I.V. Babich, E.M. Sikorski, and L.M. Gignac, "Low-voltage, scalable nanocrystal FLASH memory fabricated by templated self-assembly", IEEE 2003
[16] B.J. Kim, J.J. Chiu, G.-R. Yi, D.J. Pine, and E.J. Kramer, "Nanoparticle-Induced Phase Transitions in Diblock-Copolymer Films", Adv. Mat. 17, 2618-2622, 2005
[17] S.A. Maier, P.G. Kik, H.A. Atwater, S. Meltzer, E. Harel, B. Koel, A.A.G. Requicha, "Local detection of electromagnetic energy transmitted below the diffraction limit in metallic nanoparticle plasmon waveguides", Nature Materials, Vol. 2, April 2003
[18] J.R.Krenn, H. Ditlbacher, G. Schider, A. Hohenau, A. Leitner, F.R. Aussenegg, "Surface Plasmon micro- and nano-optics", Journal of Microscopy, Vol. 209, Pt.3 March 2003, pg167-172

Chapter 5

Materials and Experimental Methods

5.1 Introduction

This chapter presents the laboratory work done in support of this project. It lays down the practical aspects of several items that have been discussed theoretically in previous chapters. The experimental work was done under the following categories: nanoparticle synthesis, self-assembly of thin films and plasmonic waveguiding.

5.2 Nanoparticle Synthesis

Gold nanoparticles (Au NPs) were obtained by reducing chloroauric acid, $HAuCl_4$. The reducing agent, sodium citrate, also acts as a surfactant and assists, to some extent, with size control of the particles. Stock solutions of 6.0mM $HAuCl_4$ and 11.0mM sodium citrate were initially made by dissolving the required masses of acid and salt in deionized water appropriately. The DI water had a resistance of 18.6 MΩ. An important requirement for nanoparticles for plasmonic waveguiding applications is a narrow particle size distribution. To investigate narrow size distribution, an experiment to identify the optimal reactant concentrations to obtain the narrowest size distribution of the gold nanoparticles was devised. The experimental matrix consisted of sodium citrate solutions at concentrations of 2.5, 2.0, 1.5, and 1.0mM and of $HAuCl_4$ solutions at concentrations of 2.50, 2.00, 1.50, 1.25, and 1.00mM. The volume ratio of $HAuCl_4$ solution to sodium citrate solution was held constant at 10%. This is the parameter referred to as volume ratio throughout this project. UV/Vis spectra of these samples were collected and analyzed. Consequent experiments were performed on only the samples with the two highest absorption peaks from this experiment.

Next was an investigation of the effect of volume ratio. The two reactions from the experimental matrix described above were repeated at the following volume ratios: 1%, 5%, 10%, 15%, 20%, 25%, 30%, 40% and 50%. Again, two colloids were selected from this pool and used when investigating the effect of thiol capping.

A 1.0mM solution of 16-mercaptohexadecanoic acid in ethanol was used as the thiol source. Various amounts of thiol were added to the colloids and UV/Vis measurements were recorded as a function of time. At this point, it was deemed that all the parameters associated with the gold nanoparticle required before conducting the experiments on the self-assembly into thin films by the proposed methods had been obtained. Attention was thus turned to the self assembly of thin films.

5.3 Self-Assembly of Thin Films

There were two methods of self-assembled thin films explored: (a) ionic self-assembled monolayers and, which is described in Section 5.3.1, and (b) diblock copolymer self assembly, which is described in Section 5.3.2.

5.3.1. Ionic Self-Assembled Monolayers

The process of creating films by this method involved two major steps: (1) cleaning and charging the glass substrates and (2) forming the films by dipping the cleaned glass substrates into appropriate charged polyelectrolytes.

5.3.1.1 Slide Cleaning

The aim of cleaning the slides is to remove all organic residues and to build a layer of negative charge at the surface of the glass slides. This is required in order to initiate the self assembly process. The slides were initially rinsed with DI water, dried, and steeped in an acid solution called Piranha etch for 60 minutes. The Piranha etch was made by mixing 97% H_2SO_4 with 30% H_2O_2 in a 3:1 ratio. After they were exposed to the etch, the slides were removed, rinsed thoroughly with DI water, and stored under DI water. Prior to film preparation, the slides were dried by holding them in an oven at 130°C for 90 minutes.

5.3.1.2 Film Preparation

The dry slides were dipped in a polycation first, rinsed, and then dipped into a polyanion. This set of dips resulted in a polymeric coating comprised of a single bilayer on the surface of the glass slide. The polyelectrolytes used were 10.0mM solutions of poly(diallyldimethylammonium chloride) (PDDA, 100kg/mol<M_W<200kg/mol, 161g/mol repeat unit), poly(allylamine hydrochloride) (PAH, M_W = 70kg/mol, 92g/mol repeat unit), and poly (acrylic acid) (PAA, 90kg/mol). The first two polymers are polycations while the third is a polyanion and are collectively known as ionic self-assembled monomers (ISAMs). The carboxylic end group on the thiol-functionalized acid used for thiol capping of the gold nanoparticles causes the capped nanoparticles to be negatively charged. The resulting colloidal solution acts as a polyanion. It is this interaction which was explored to self-assemble a sheet of the gold nanoparticles into the polymer films. Films were created with either 1 or 5 bilayers composed of various combinations of polyelectrolytes and thiol-capped gold nanoparticles. Atomic force microscopy (AFM) images were obtained for the single bilayer films while UV/Vis absorption measurements were made on the 5 bilayer films. Films with about 2.5 quadlayers were also produced.

In order to create the bilayers, PAH, PAA, and the thiol-capped nanoparticles were used. In preliminary experiments, PDDA was found to cause agglomeration of the gold nanoparticles and was therefore not used in films with gold nanoparticles. Fig.5.1(a)

illustrates the dipping sequence, beginning with PAH and followed by rinsing, dipping in the thiol-capped gold colloid and then rinsing again. After each rinse, the excess water was allowed to air dry in ambient room conditions before the next layer was deposited. Each dipping time lasted five minutes.

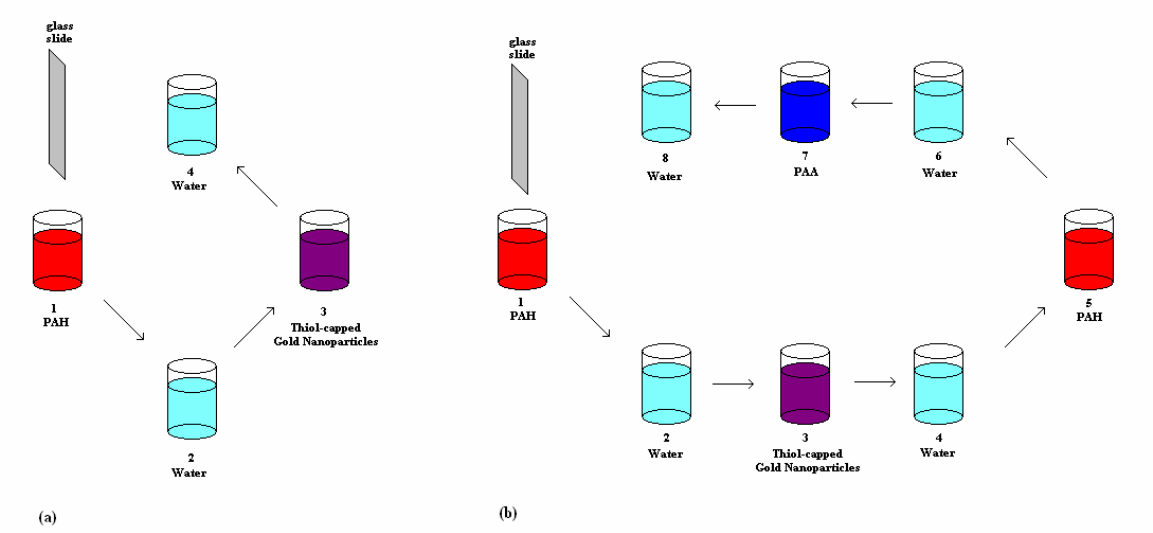

Fig.5.1 ISAM Dipping Sequence for (a) a single PAH/Au NP bilayer, and (b) a single PAH/Au NP/PAH/PAA quadlayer

The quadlayer films were made in a similar fashion with the only change being an extra PAA layer in between gold nanoparticle layers (Fig.5.1(b)). All dipping times were 5 minutes except when dipping the glass slides into the gold nanoparticles. These were dipped for 10 minutes to ensure nanoparticle attachment. Dipping was achieved by securing the glass slides in a holder, attaching it to a three-axis adjustable mount and lowering it into the solution. After the allotted amount of time, the slides were raised and allowed to dry.

5.3.2 DiBlock Copolymer Self-Assembly

This process involved spin coating a micellar diblock copolymer solution onto a glass substrate. The copolymer used was polystyrene-b-poly(2-vinyl pyridine), (PS-b-P2VP, 190 kg/mol-b-190 kg/mol; PDI = 1.10, Polysciences Inc). 0.1 grams of the solid diblock copolymer was dissolved in toluene to give a 10.0 wt% solution from which 0.5 and 0.1 wt% solutions were made. Drops of these solutions were spun coated onto substrates to for 15, 30 and 60 seconds at 2000 rpm to create thin films. This experimental matrix enabled the investigation of phase separation of the micellar solution under variations in concentration and spin coating time.

It has been reported that the P2VP block forms complexes with metals and solutions of metals [1]. To investigate the usefulness of this for our purposes, two 0.1ml aliquots of 0.1 wt% micellar solution were measured out. Added to the first was 0.1 ml of $HAuCl_4$ and to the other, 0.1ml gold colloid. Both resulting solutions were shaken thoroughly for two minutes and allowed to settle for about five minutes. Drops of the resulting toluene

partition were spun coated onto glass slides. A few drops of each of the mixtures were also deposited onto glass slides and the water and toluene were allowed to evaporate. AFM images of these slides were taken to adjudge which method best gave some semblance of a suitable arrangement of gold nanoparticles.

5.4 References

[1] B.-H. Sohn, J.-M. Choi, S.I. Yoo, S.-H. Yun, W.-C. Zin, J.C. Jung, M. Kanehara, T. Hirata, and T. Teranishi, "Directed Self-Assembly of Two Kinds of Nanoparticles Utilizing Monolayer Films of Diblock Copolymer Micelles", J. Am. Chem. Soc. 123, 6368-6369, 2003

Chapter 6

Results and Discussion

6.1 Introduction

This chapter discusses the results of the experiments described in Chapter 5. It also provides some justification as to the direction chosen for consequent experiments. In some cases, other results that support or dispute these results are mentioned and discussed.

6.2 Nanoparticle Synthesis

The colloids created were investigated by means of UV/Vis absorption spectroscopy in which features of the surface plasmon resonance (SPR) peak were measured and by transmission electron microscopy (TEM) in which the physical dimensions of the nanoparticles were measured. While the SPR measurements yielded information on the frequency response of the colloids to electromagnetic excitation, the TEM measurements provided data on the exact dimensions of the particles.

The spectra of surface plasmon resonance peaks obtained from the reactions of several different concentrations of $HAuCl_4$ (denoted by a specific number) and sodium citrate (henceforth referred to as NaCitrate) (denoted by a specific letter) are given below (Fig.6.1 and Fig.6.2). The NaCitrate solution concentrations used were 2.5, 2.0, 1.5, and 1.0mM while the $HAuCl_4$ solution concentrations used were 2.50, 2.00, 1.50, 1.25, and 1.00mM.

Table 6.1 Key for $HAuCl_4$:NaCitrate Reaction Matrix

		NaCitrate Concentration			
$HAuCl_4$ Concentration		2.5mM	2.0mM	1.5mM	1.0mM
	2.50mM	a1	b1	c1	d1
	2.00mM	a2	b2	c2	d2
	1.50mM	a3	b3	c3	d3
	1.25mM	a4	b4	c4	d4
	1.00mM	a5	b5	c5	d5

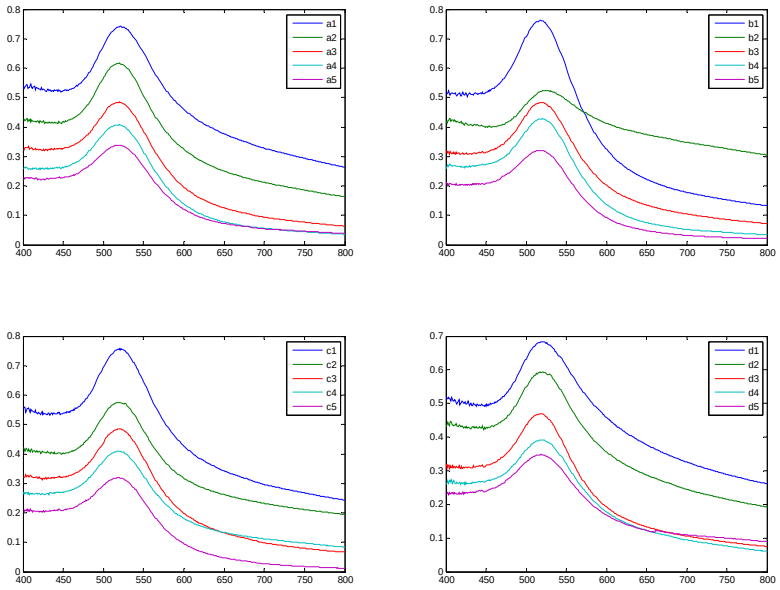

Fig.6.1 Absorption spectra of the SPR peak from gold nanoparticles illustrating effect of varying $HAuCl_4$ concentrations at constant NaCitrate concentrations

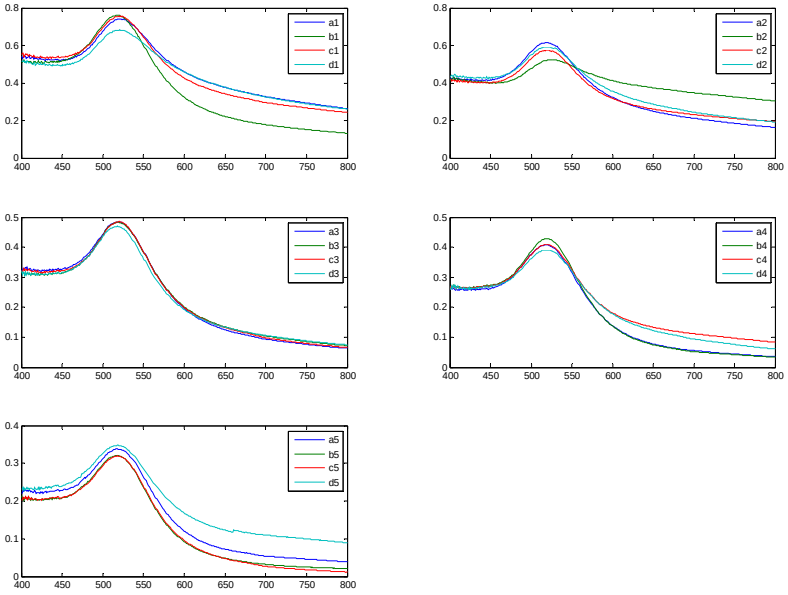

Fig.6.2 Absorption spectra of the SPR peak from gold nanoparticles illustrating effect of varying NaCitrate concentrations at constant $HAuCl_4$ concentrations

As can be seen in Figs. 6.1, increasing the chloroauric acid concentration resulted in larger gold particles, confirmed by the slight red shift in the SPR peak wavelength at higher $HAuCl_4$ concentrations. From Figs. 6.1 and 6.2, colloids b1 and c1, corresponding to reactions between 2.5mM $HAuCl_4$ and 1.5 and 2.0mM NaCitrate, respectively, were

chosen for further experimentation since the absorption curves associated with the gold nanoparticles produced via these reactions produced the highest peak-to-FWHM (full-width-half-maximum) ratios of all the reactions. In Fig.6.3, there are two plots showing the peak-to-FWHM ratios across all the reactions in Table 6.1 by both $HAuCl_4$ and NaCitrate concentration.

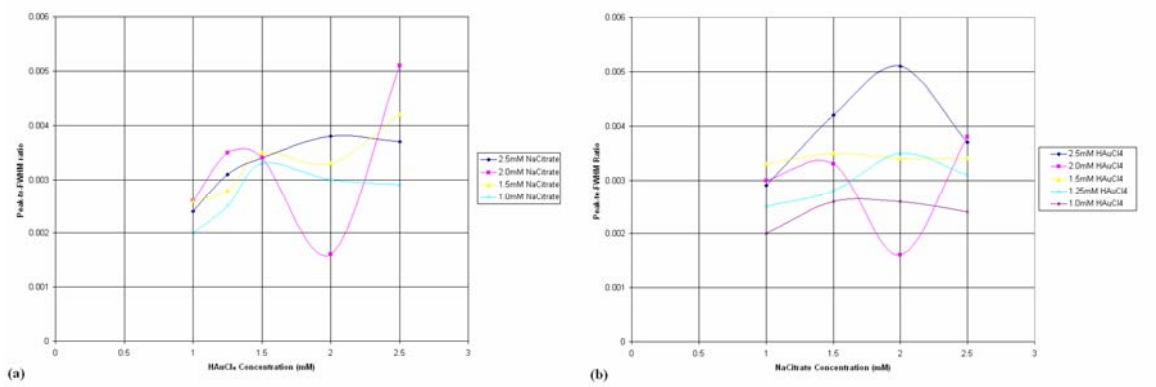

Fig.6.3 Peak-to-FWHM ratios of reactions in Table 6.1 by (a) NaCitrate concentration, and (b) $HAuCl_4$ concentration

Both plots justify why reactions b1 and c1 were selected even though the trends in the reactions are empirical and not clearly obvious. The FWHM was calculated by assuming that the only responses in the absorption spectra were due to surface plasmon peaks between 520 and 540 nm and were of Gaussian distributions. The end points were therefore assumed to satisfy the Rayleigh scattering criterion,

$$I \propto \frac{1}{\lambda^4} \qquad (6.1)$$

and the endpoints of the spectra were therefore fitted to

$$I = a\frac{1}{\lambda^4} + b \qquad (6.1)$$

by way of a Matlab® program. The constants *a* and *b* are assumed to be arbitrary for each absoption spectrum and only assisted with obtaining the FWHM. While *a* served to scale the absorption spectra appropriately, *b* aided with adjusting the baseline offset, which is introduced by the electronics associated with the spectrometer. The maxima for the absorption curves were read off the plots and the peak-to-FWHM ratios were determined and plotted to obtain Fig.6.3.

The absorption spectra of the nanoparticles synthesized using reactions b1 and c1 were also compared to the absorption spectra predicted by theory (Equation 2.32) for gold particles of approximately 10 nm diameter surrounded by water (n=1.33) and the resulting plots are in Fig.6.4.

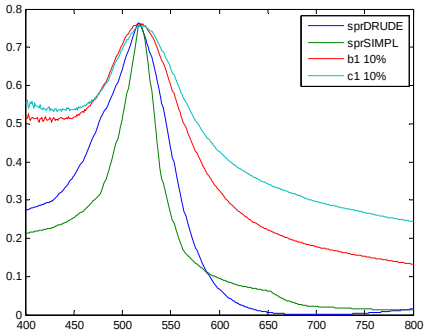

Fig.6.4 Comparison of theoretical and experimental absorption curves for Au NPs in water

Two theoretical absorption spectra are shown for which different calculation methods were employed. The spectra labeled 'sprSIMPL' was calculated directly using refractive index (n) and extinction coefficient (k) data taken from [1] and the spectra labeled 'sprDRUDE' was calculated by taking into consideration the Drude theory of free electron metals. The kinks in the computed spectra are due to extrapolation between data points given in [1]. The spectrum for 'sprSIMPL' is narrower than the others and this is because its model (Equation 2.32) assumes a single particle is excited. The Drude model spectrum is more realistic.

Subsequent to the selection of reactions b1 and c1, the effect of volume ratio was investigated next. The reactions b1 and c1 had been selected from reactions performed at volume ratios of 10%. Table 6.2 provides information on the volumes used in this experiment.

Table 6.2 Actual reaction volumes for experiments investigating effects of volume ratio

Volume Ratio	1%	5%	10%	15%	20%	25%	30%	40%	50%
Colloid b1									
2.0mM NaCitrate (ml)	10	6	6	6	6	6	6	6	6
2.5mM $HAuCl_4$ (ml)	0.1	0.3	0.6	0.9	1.2	1.5	1.8	2.4	3
Colloid c1									
1.5mM NaCitrate (ml)	10	6	6	6	6	6	6	6	6
2.5mM $HAuCl_4$ (ml)	0.1	0.3	0.6	0.9	1.2	1.5	1.8	2.4	3

The data from these experiments in which the ratio of the volume of $HAuCl_4$ solution to the volume of NaCitrate solution was varied is given below in Fig.6.5 and Fig.6.6.

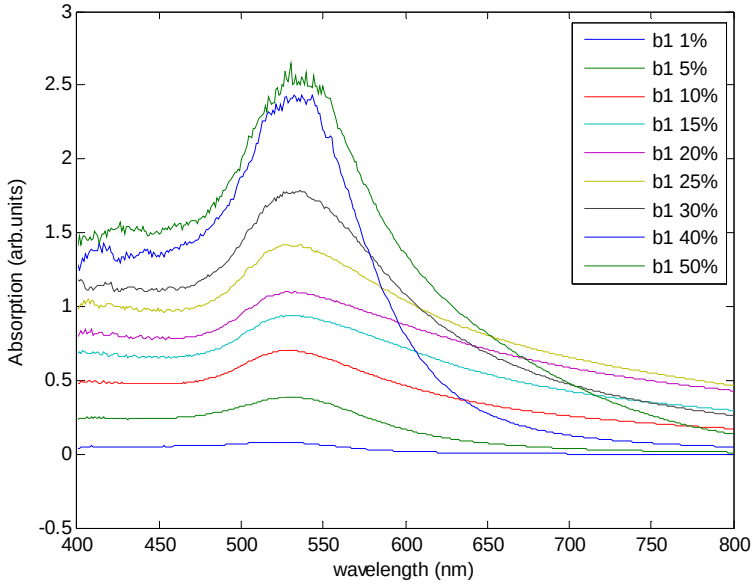

Fig.6.5 Effects of varying volume ratio on the SPR peak of Au NPs synthesized using reaction b1

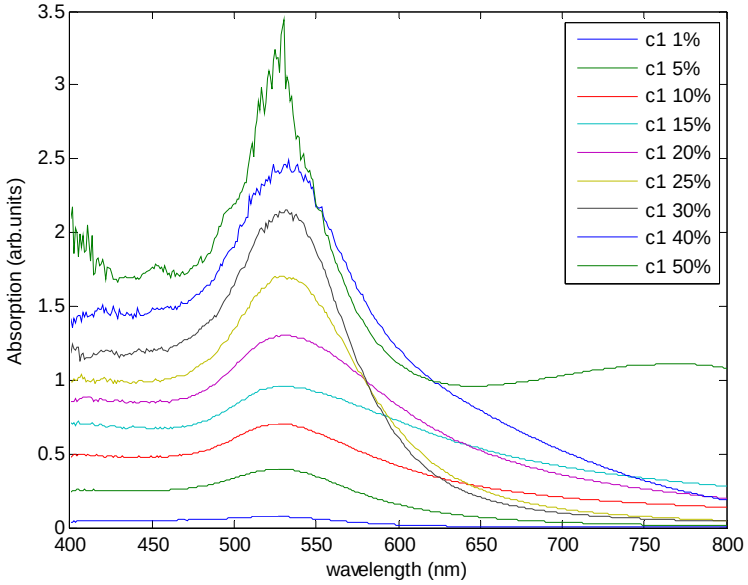

Fig.6.6 Effects of varying volume ratio on the SPR peak of Au NPs synthesized using reaction c1

As the volume ratio increased, the number of particles in solution increased obviously due to the increasing amounts of reactants. At volume ratios of 30% and above, however, the absorption peaks began to show significant sensitivity to noise due to the low level of light that is transmitted through the samples. The absorption spectrum of reaction c1 at a volume ratio of 50% was quite unique. Apart from a much higher absorption peak, it was also much narrower than all the rest. This would suggest a marked increase in the uniformity of the particle size distribution at this volume ratio. Some agglomeration of particles was also observed, suggested by the increase in the response of this sample (c1 50%) between 650-800nm. As a fine balance between the two extremes, particles with a

20% volume ratio were consequently selected for the project. TEM images of reaction b1 at volume ratios of 10% and 20% are given in Fig.6.7. Some amount of size and shape variations was present with increased volume ratio. As mentioned earlier in Chapters 2 and 3, such variation in particle shape and size introduce performance losses into plasmonic waveguide operation. The size variation results in the broadening of the range frequencies that can propagate along such a waveguide as particles of different sizes have different resonant frequencies. This difference in resonant frequencies can lead to similar dispersion effects seen in single and multimode optical fibers. Apart from size related effects, particles of different shapes can introduce other frequencies corresponding to various axes of vibration within the particle. Nanorods and ellipsoid-shaped nanoparticles are known to resonate with often two and sometimes three frequencies, corresponding to their various axes.

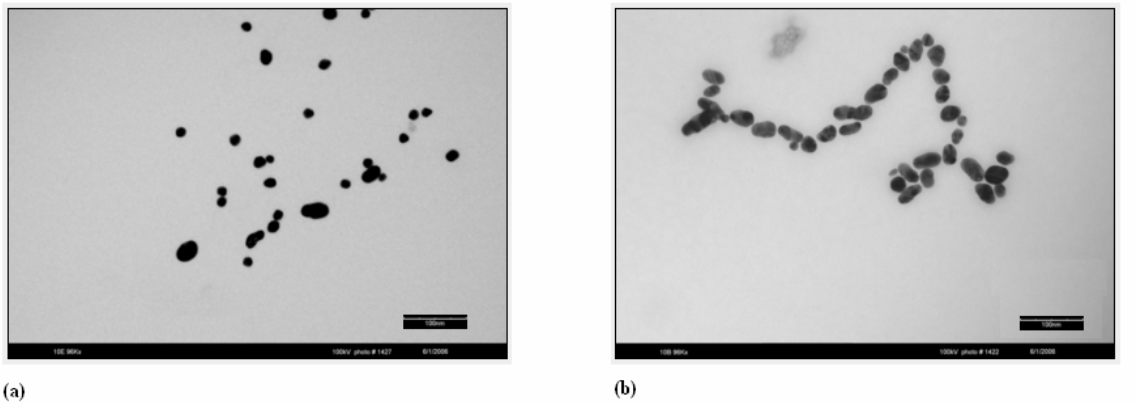

Fig.6.7 TEM Image of Au NPs formed by reaction b1 at volume ratio (a) 10%, and (b) 20%. The increase in average particle size due to the higher $HAuCl_4$ concentration is clearly visible. The scale bars in the bottom right corners represent 100nm lengths.

In order to facilitate assembly into thin films, thiol capping was investigated next. Absorption spectra of the thiol capped nanoparticles were recorded from initial addition of thiol until 192 hours later and are given in Fig.6.8. Significant drops in the absorption peaks of the gold colloids immediately after thiol addition were observed. This is very likely a result of the change in the effective refractive index in the immediate vicinity of the nanoparticles as the thiol groups bind to their surfaces.

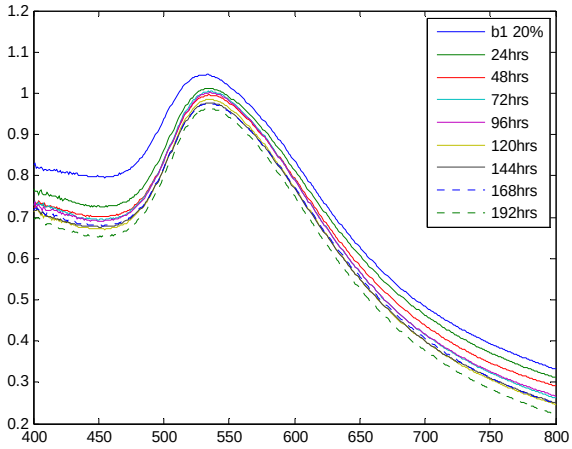

Fig.6.8 Effect of time on thiol-capped Au NPs produced by reaction b1 at volume ratio 20%. The change in refractive index in the immediate vicinity of the nanoparticles causes a red-shift in the SPR spectra. Over time the SPR spectra amplitude falls.

For colloid b1, the absorption peaks continued to drop gradually, but at a reducing rate, over time, as shown in Fig.6.8. However, for colloid c1, the absorption peak rose in the opposite direction but settled eventually (Fig.6.9). The only significant difference between these experiments, apart from sample, was the difference in the amount of alcohol relative to thiol and nanoparticle sample. This thus seemed to have depended on the amount of alcohol used as a mixing agent between the aqueous phase of the colloid and the alcohol phase of the thiol. This was not investigated any further.

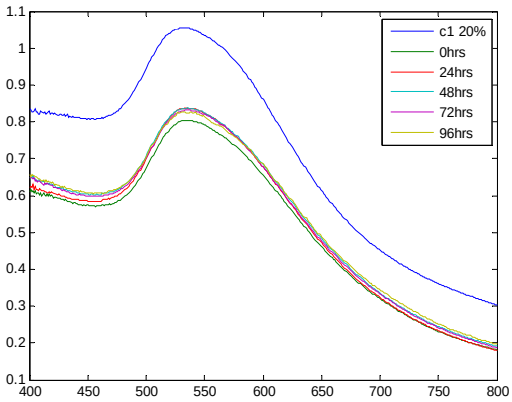

Fig.6.9 Effect of time on thiol-capped Au NPs produced by reaction c1 at volume ratio 20%. The change in refractive index in the immediate vicinity of the nanoparticles causes a red-shift in the SPR spectra. Over time the SPR spectra amplitude rises.

6.3 Self-Assembly of Thin Films

The characterization of the thin films involved SPR and AFM measurements. While the SPR spectra were analyzed to investigate that interaction between the nanoparticles arising from their fixed positions in a film, the AFM measurements were collected to provide a two-dimensional image of how the particles aligned themselves in the thin films.

6.3.1 Ionic Self-Assembled Monolayers (ISAMs)

Single-bilayer ISAMs were primarily used to obtain AFM images of the arrangements of thiol-capped gold nanoparticles in polymer films. As a preliminary test, a measurement of the surface of a glass/PAH/PAA/PAH/PAA/PAH/thiol-capped gold nanoparticles (b1,20%)/PAH was imaged and is shown in Fig.6.10.

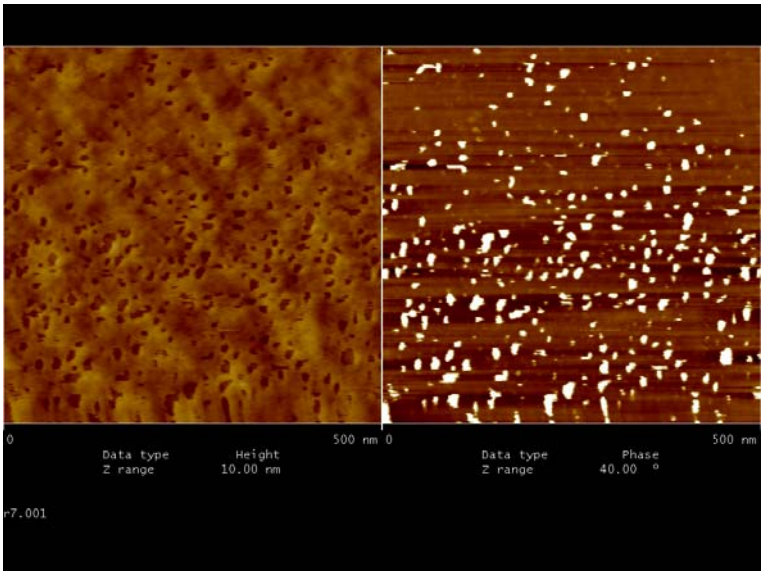

Fig.6.10 AFM of PAH-covered thiol-capped nanoparticle film. Particle arrangement is random. Dips are typically small single particles.

The particle arrangement is highly random. While varying heights would have been expected, the image seemed to have been dominated by dips instead. The dips are approximately 10nm in depth which is on the order of the sizes of the particles. More dips can be seen in the lower part of the picture as compared to other areas and, therefore, suggests that particles may not be adhering uniformly to the film.

ISAMs with several bilayers were used to investigate plasmonic waveguiding. Formed in the manner described in Section 5.3.1, ISAM films would be expected to be composed of sheets of nanoparticles with controllable polymer thicknesses between sheets. Varying these distances, by altering the number of layers of polycations and polyanions in the stack, provides a means to form a large waveguiding structure with controlled spacing in a given direction. Two films were created, one with 5 bilayers of the repeat bilayer PAH/thiol-capped b1 nanoparticles and the other with 2.5 quadlayers of the repeat quadlayer PAH/thiol-capped c1/PAH/PAA. The resulting UV/vis spectra recorded as these films were being made are given in Fig.6.11 and Fig.6.12.

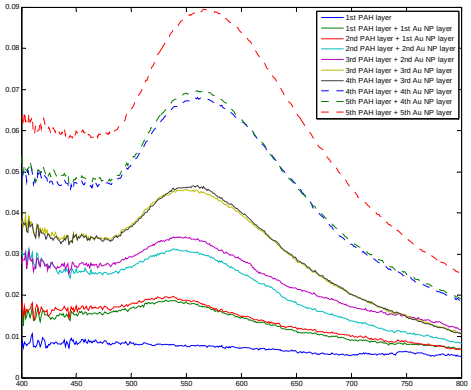

Fig.6.11 SPR spectra of 10 layer PAH/thiol-capped Au NP film. The increasing red-shift and amplitude magnitude increase in the spectra as more layers are added demonstrates the effect of near field interactions necessary for plasmonic waveguiding.

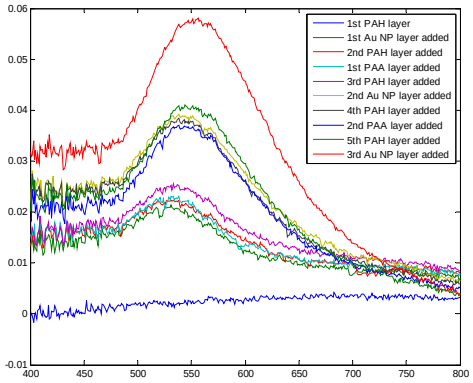

Fig.6.12 SPR spectra of 10 layer PAH/thiol-capped Au NP/PAH/PAA film. Larger spacing between polymer layers results in reduced near field interations.

There is a clear difference in the rates of lateral shift of the absorption peaks with regards to the number of layers. In Fig.6.11, the Au NP layers are much closer, which gives rise to a larger wavelength shift in the SPR peak since their electric near fields interact more strongly. In the other film, the larger spacing between the particles leads to a much reduced lateral wavelength shift in the absorption peaks. The larger the spacing between particles, the smaller is the shift from the absorption spectrum expected for individual isolated particles in the same dielectric. Another interesting observation is the fact that the absorption spectra representing the first Au NP layers in both films suggest that the particles in both films are somewhat isolated. Combining these two facts, one can infer that the effective intra-layer coupling between particles may be smaller than the inter-layer coupling.

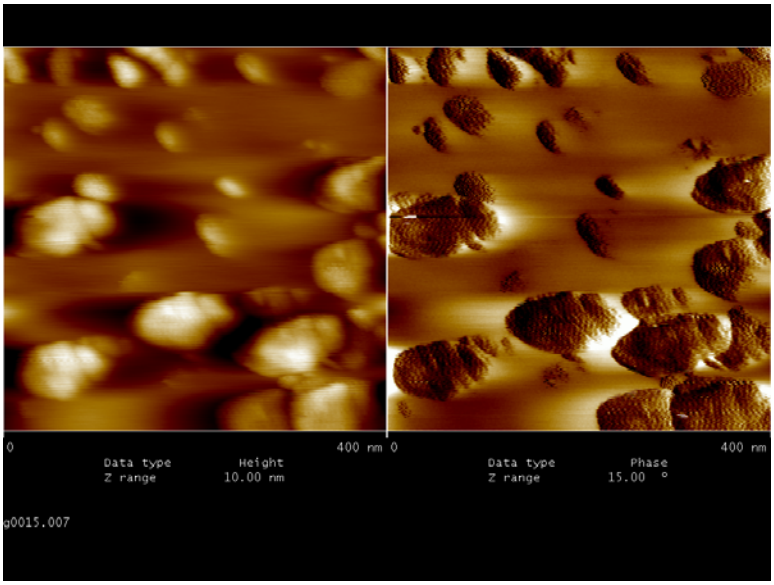

Fig.6.13 AFM image of film B. Image on left shows areas with assemblies of nanoparticles much larger than in Fig.6.10. Careful observation reveals that particles in these assemblies are isolated.

As a crosscheck on intra-layer particle coupling, a single bilayer (Fig.6.13) was formed by immersing the sample in the gold colloid for a long time (20hrs). The resulting absorption spectrum is given in Fig.6.14, where it is compared with the multilayer film formed with the same polycation (PAH) and gold colloid (b1,20%).

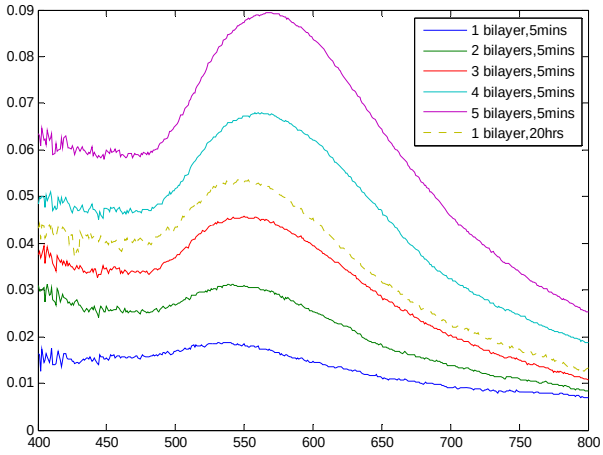

Fig.6.14 Illustrating effect of dipping time on film formation. Increased dipping time for a single layer results in increased near field interactions.

Compared to the single film dipped for 5 minutes (henceforth called Film A), the 20hr single film (henceforth called Film B) has a higher magnitude SPR peak which is red-shifted from that of Film A. The increase in the SPR peak magnitude suggests that there are more particles on the film, a logical deduction since there is more time for particles to settle on it. The red shift of the SPR peak suggests that the particles are packed closer together in Film B than in Film A. However, unlike reported by Hemtanon [2], no peaks attributable to agglomeration were observed and this, therefore, suggests that the red-shift was due to near field interactions of the many more particles that settle on the film in 20hrs than in 5minutes. If agglomeration were observed, it would suggest that the particles were sticking together and therefore near field interactions alone would not be enough to explain the red-shift. This suggests that, while self-assembly might be almost instantaneous for molecules as suggested by McAloney [3], nanoparticles, which are a little more massive, may take longer to self-assemble. Forming layers for 20hrs may, however, prove impractical unless waveguiding is performed in the plane in which the gold particles assemble.

Applying the same model Brongersma [4] applied to 25nm radius Ag particles spaced 75 nm apart in air to the gold nanoparticles used for the films in this project, we have

$$N_e = \frac{4}{3}\pi r^3 \frac{L\rho}{M}, \qquad (7.1)$$

which gives $N_e = 2.858\text{x}10^5$ electrons for particles of diameter 21nm, which is an approximate average for the gold nanoparticles used in the films. For gold particles below 25nm, the intrinsic size regime applies and, hence, it is safely assumed that all the electrons in the particle participate in the oscillation.

Table 6.3 Comparing effect of time on single bilayer self-assembled films

Deposition Time	Resonance wavelength (nm)	Resonance Peak (arb. units)
5 mins	532±1	0.01880
20 hrs	548±1	0.05377

While Equation 3.3 cannot be applied directly, the information in Table 6.3 gives us an idea of the intra-layer coupling between the particles. In solution, the nanoparticles used had a resonant wavelength of approximately 532nm. This suggests that there was sparse deposition of the nanoparticles in Film A, but that the spacing between nanoparticles is much smaller in Film B. Analyzing this data using Equations 3.3 and 3.5, it can be shown that the absorption peak shifts to 548nm for a distance of about 43 nm. Transverse oscillations are assumed since the only possible out-of-plane excitation is transverse (Fig.6.15). The refractive index of the polycation, PAH, was taken to be 1.52 [5].

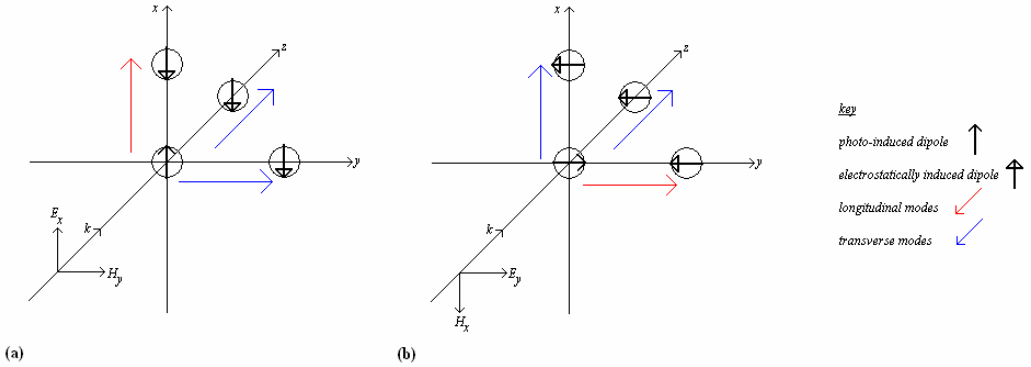

Fig.6.15 Illustration of transverse and longitudinal modes for (a) electric field along x, and (b) electric field along y

Therefore we assume that the average spacing between particles in Film B is about 43nm (Fig.6.16). Thus the absorption data demonstrates that plasmonic waveguiding can be achieved within the film.

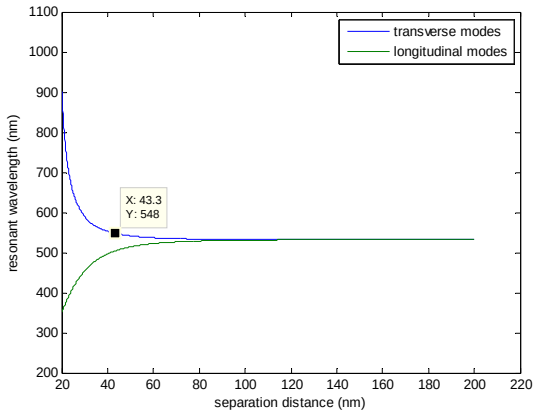

Fig.6.16 Effect of average separation distance and frequency shift for Film B. Near field coupling increases with decreasing particle separation.

The coupling strength parameter, $\omega_1 \approx 6.4\text{x}10^{14}$, is on the order of the angular velocity of the incident light, $\omega_o \approx 3.5\text{x}10^{15}$, confirming strong intra-layer interaction at this average separation.

6.3.2 DiBlock Copolymer Self-Assembly

As described in Section 5.3.2, diblock copolymer films were deposited on glass substrates by spin coating and by evaporation. An overriding requirement in diblock copolymer self-assembly is the thickness of the films created. These two methods were expected to give different film thicknesses which would then vary the process by which self-assembly would depend.

An AFM image of a 0.5wt% solution of PS-b-P2VP spun cast for 15 seconds is given in Fig.6.17.

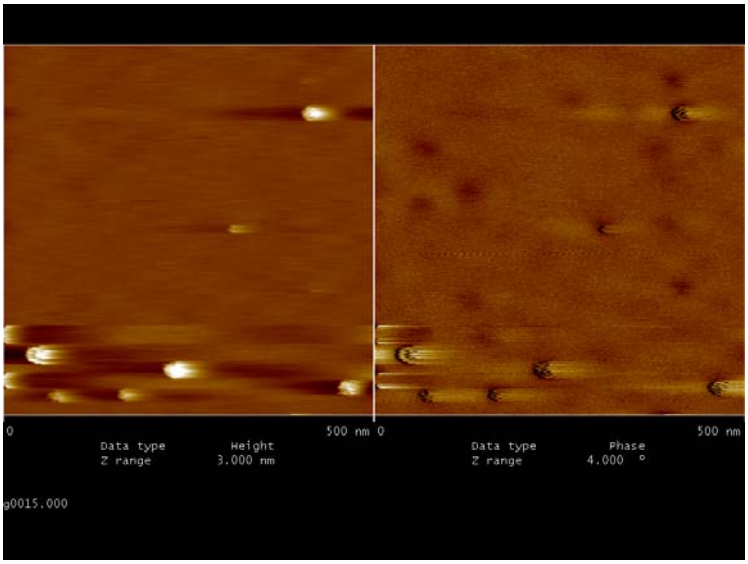

Fig.6.17 Atomic Force Microscope image of a spin cast solution of 0.5wt% PS-b-P2VP. Phase separation affected by an extremely thin layer of film, approximately 3nm thick at thickest points.

The film shows little phase separation. The maximum height of the film is 3nm. The absence of any phase separation at this height would suggest that the required thickness for diblock copolymer self-assembly to occur at, the intrinsic polymer length scale, is larger than 3nm. In contrast, isolated lamellar structures were observed to have formed in certain portions of a film made by evaporation with the same solution (Fig.6.18). These structures have heights of about 25nm and widths of approximately 6.5nm.

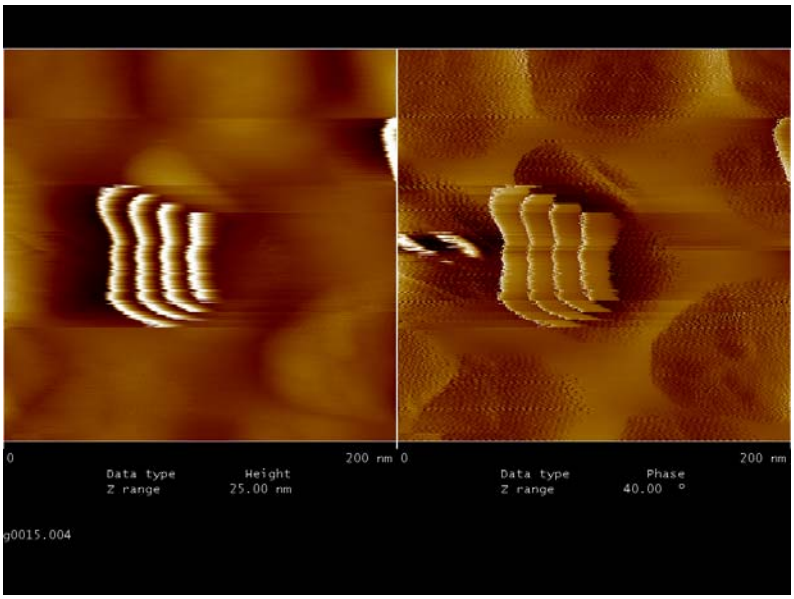

Fig.6.18 Atomic Force Microscope image of an evaporated solution of 0.5wt% BCP. Isolated lamellar nanostructures were observed with height 25nm and width 6nm.

Surrounding these structures were areas with some height variation. However, there was insufficient polymer to support self-assembly as seen in the center if this image. The lamellar structures were found in several locations on the film but never as a continuous structure larger than about 60nm along the lamellae. Some possible reasons for the inconsistency in this film might be due to non-uniform evaporation of the solvent, toluene, and potentially the nanoscale roughness of the glass substrate surface.

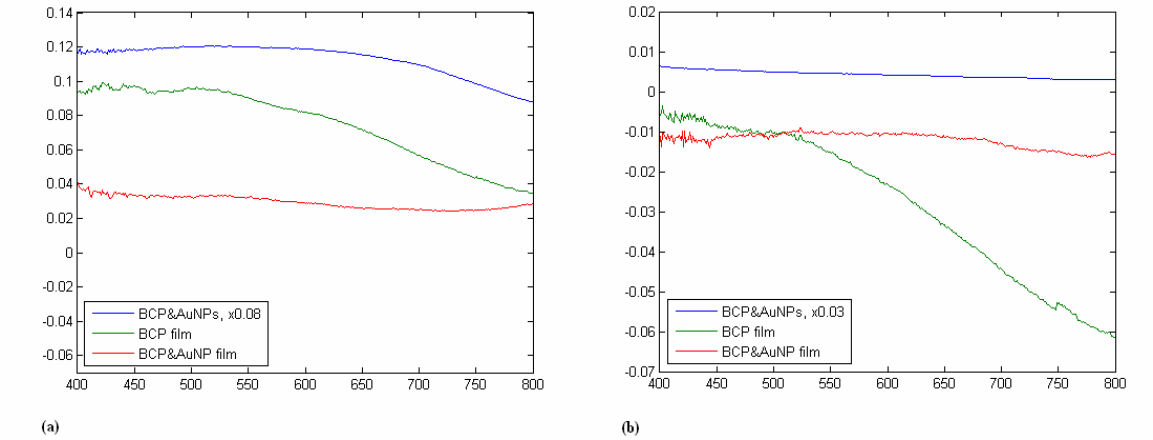

Fig.6.19 UV/Vis absorption spectra of PS-b-P2VP diblock copolymer thin films with concentration (a) 0.5wt% (b) 0.1wt%. Particles show aggregation in solution (blue plots) and this worsens when evaporated onto a film (red plots).

UV/Vis absorption spectra were measured for evaporated diblock copolymer films that contained gold nanoparticles. For both concentrations used, 0.1wt% and 0.5wt%, some amount of agglomeration was observed in solution which got worse with evaporation onto a glass substrate (Fig.6.19). A possible explanation for these results is that the reactions between the P2VP core and gold nanoparticles may be sufficiently strong that particles are brought into contact around these cores. This would result in an increase in

the effective size of the metal structure in which the surface plasmons are induced (and therefore giving an absorption spectrum with a reduced amplitude and a red-shifted absorption peak) as well as a physical contact between the individual nanoparticles which would negate the ability of localized surface plasmons to be propagated from one particle to another. Particle aggregation was more pronounced in the film with the higher diblock copolymer concentration, suggesting that larger masses of agglomerated nanoparticles may be occurring with the presence of more P2VP sites. These observations do not bode well for demonstrating plasmonic waveguiding action.

6.4 References

[1] http://www.ioffe.rssi.ru/SVA/NSM/nk/Metals/Gif/au.gif

[2] B. Hemtanon, H.C. Warad, A. Sugunan, C. Thanachayanont, and J. Dutta, "Novel thin film deposition of colloidal nanoparticles", Proceedings of the International Conference on Smart/Intelligent Materials, SmartMat-'04, December 1-3, 2004, Chiang Mai, Thailand, (ISBN 974-656-288-8) pp. 194-196.

[3] R.A. McAloney and M.C. Goh, "In Situ Investigations of Polyelectrolyte Film Formation by Second Harmonic Generation", J. Phys. Chem. B, 103, 10729-10732, 1999

[4] M.L Brongersma, J.W. Hartman, H.A. Atwater, "Electromagnetic energy transfer and switching in nanoparticle chain arrays below the diffraction limit", Phys Rev B, Vol. 62, No. 24, December 2000

[5] S.E. Burke and C.J. Barrett, "Swelling Behavior of Hyaluronic Acid/Polyallylamine Hydrochloride Multilayer Films", Biomacromolecules, 5, 1419-1428, 2005

Chapter 7

Conclusion

7.1 Suggestions for Future Work

There are several interesting issues that this work leaves unexplored, but will need to be addressed at some point in the future if plasmon waveguide structures are to be fully realized by the processes investigated in this project. These include improvements to nanoparticle uniformity in size and shape and further work on waveguide fabrication and characterization.

7.1.1 Nanoparticle Synthesis Improvements

In this work, while some attention was paid to obtaining the best nanoparticles for the waveguide application under the circumstances, the TEM images obtained on the nanoparticles used during this project clearly shows that the synthesis of monodisperse nanoparticles was not always attained. The differences in size and shape in nanoparticles that are not monodisperse introduce differences in the charge build up around the nanoparticles. This negatively affects the self assembly process since adjacent particles see different forces due to the charged layers and, hence, uniformity in a self-assembled layer is compromised.

Several other methods for making nanoparticles exist and may be explored with the aim to improve particle uniformity. Some of these methods include reduction of $HAuCl_4$ by $NaBH_4$ and even making metallic nanoparticles composed of other materials like silver or aluminum. An interesting idea would be to investigate methods to produce nanoparticles from magnetic metals where their assembly can be assisted by magnetic fields.

7.1.2 Waveguide Fabrication and Characterization

With the self-assembled films demonstrated in this work, suitable waveguiding structures could be patterned and investigated from these films by means of photolithography as a logical follow up to this project. A single film with a sufficient nanoparticle density should suffice as a substrate from which plasmonic waveguides can be etched. Alternatively, multi-layer films may be used with the etching done so that waveguiding structures are either parallel (like with a single film) or perpendicular (Fig.7.1) to the direction in which the self-assembled layers are stacked. Once fabricated, the waveguides would be characterized to investigate typical waveguide properties like loss, dispersion, bandwidth and other parameters common to waveguides in general.

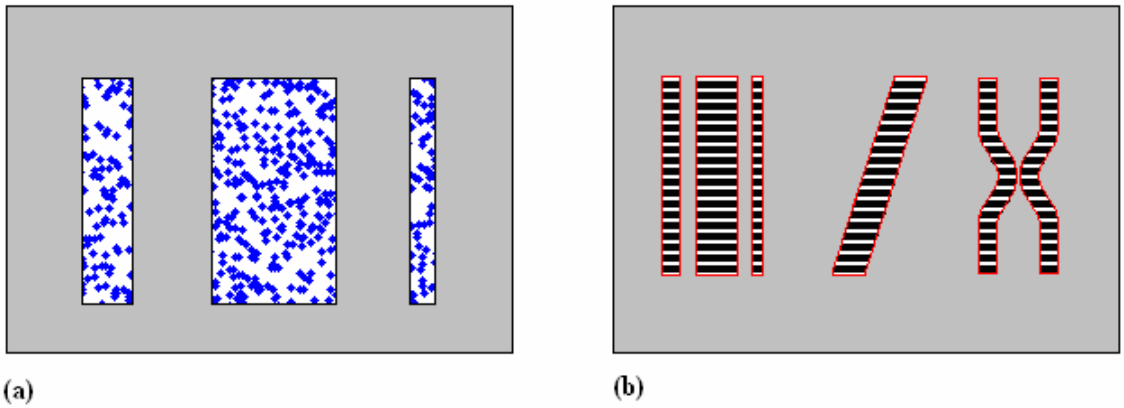

Fig.7.1 Illustration of plasmonic waveguides etched from a thin film of (a) nanoparticles on a single layer, and (b) sheets of nanoparticles along the direction of the layers.

Means for exciting such waveguides were discussed earlier; such waveguides could be integrated initially with standard semiconductor processes to facilitate data routing around chips. Later on they may find use for performing simple control [1] and logic operations [2], and application in integrated optical circuits [3].

7.2 Comparison of ISAM and Diblock Copolymer Self Assembly

In general, these two methods each have advantages and disadvantages to their use. For instance, both processes do not require many expensive steps to produce. ISAMs are easily made by hand or mechanical dipping in water soluble polymers. Diblock copolymer films are easily deposited by either evaporation or spin coating, common methods in use.

However, ISAM self-assembly, which is a fast process when applied to molecules, may take some a while to assemble if high coverage is needed in a single layer. This is beneficial if waveguides are to be etched from a single layer but it may take up significant manufacturing time. Particle placement is also highly random even though this may be circumvented by using highly uniform particles on a film with high coverage. Diblock copolymers on the other hand typically leave one exposed to strong organic solvents, which are required to dissolve the diblock copolymer (e.g. toluene, cyclohexane, tetrahydrofuran, etc). Another critical parameter, which may be difficult to control, is evaporation rate of these solvents. This may have contributed significantly to the incoherency in diblock copolymer films in this project.

Based on the work done in this project, ISAM films would be recommended as a preferred choice for future work. Against that backdrop, however, if a means of improving the area consistency self-assembly of diblock copolymers at the nanoscale are found, along with a means of enforcing separation between particles, they may indeed prove superior to ISAMs in the long run.

7.3 Conclusion

This project sought to demonstrate the suitability of colloidal nanoparticles for use in plasmonic waveguides. Work was undertaken in the areas of nanoparticle synthesis and thin film preparation. It was shown that nanoparticles can be grown and their surfaces modified to improve their surface chemistry and facilitate the self-assembly process. The results discussed in Chapter 6 suggest that it is possible to self-assemble these particles into polymer thin films to form structures that lend themselves to plasmonic waveguiding. The fabrication of plasmonic waveguides from such films would be much cheaper and easier to produce than by the alternate means of electron beam lithography, atomic force microscopy, scanning near field optical microscopy or dip-pen lithography. One of the major downsides to this method is the loss in precision achievable with these more expensive methods. However, with improvements in material and processing parameters, such differences should be reducible to a bearable minimum.

7.4 References

[1] A.V. Krasavin, K.F. MacDonald, N.I. Zheludev, A.V. Zayats, "High-contrast modulation of light with light by control of surface plasmon polariton wave coupling", Appl. Phys. Lett., Vol. 85, No. 16, October 2004

[2] J. Tominaga, C. Mihalcea, D. Buchel, H. Fukuda, T. Nakano, N. Atoda, H. Fuji, T. Kikukawa, "Local Plasmon photonic transistor", Applied Physics Letters, Vol. 78, No 17, April 2001

[3] M. Hochberg, T. Baehr-Jones, C. Walker, and A. Scherer, "Integrated Plasmon and dielectric waveguides", Optics Express 5481, Vol. 12, No. 22, 5481, November 2004